Naval Research Laboratory

Washington, DC 20375-5320

NRL/MR/6410--98-8190

Numerical Modeling of Fire Suppression Using Water Mist. 3. Methanol Liquid Pool Fire Model

KULDEEP PRASAD*
CHIPING LI
K. KAILASANATH

Center for Reactive Flow and Dynamical Systems
Laboratory for Computational Physics and Fluid Dynamics

CHUKA NDUBIZU**
RAMAGOPAL ANANTH
P.A. TATEM

Naval Technology Center for Safey and Survivability
Chemistry Division

*Science Application International Corporation, VA
**Geo-Centers Inc., MD

October 30, 1998

DTIC QUALITY INSPECTED 4

19981116 054

REPRODUCTION QUALITY NOTICE

This document is the best quality available. The copy furnished
to DTIC contained pages that may have the following quality
problems:

- Pages smaller or larger than normal.

- Pages with background color or light colored printing.

- Pages with small type or poor printing; and or

- Pages with continuous tone material or color
  photographs.

Due to various output media available these conditions may or
may not cause poor legibility in the microfiche or hardcopy output
you receive.

☒ If this block is checked, the copy furnished to DTIC
contained pages with color printing, that when reproduced in
Black and White, may change detail of the original copy.

REPORT DOCUMENTATION PAGE

Public reporting burden for this collection of information is estimated to average 1 hour per response, including the time for reviewing instructions, searching existing data sources, gathering and maintaining the data needed, and completing and reviewing the collection of information. Send comments regarding this burden estimate or any other aspect of this collection of information, including suggestions for reducing this burden, to Washington Headquarters Services, Directorate for Information Operations and Reports, 1215 Jefferson Davis Highway, Suite 1204, Arlington, VA 22202-4302, and to the Office of Management and Budget, Paperwork Reduction Project (0704-0188), Washington, DC 20503.

1. AGENCY USE ONLY (*Leave Blank*)	2. REPORT DATE October 30, 1998	3. REPORT TYPE AND DATES COVERED NRL Memorandum Report

4. TITLE AND SUBTITLE

Numerical Modeling of Fire Suppression Using Water Mist. 3. Methanol Liquid Pool Fire Model

5. FUNDING NUMBERS

6. AUTHOR(S)

Kuldeep Prasad,* Chiping Li, K. Kailasanath, Chuka Ndubizu,** Ramagopal Ananth, and P.A. Tatem

7. PERFORMING ORGANIZATION NAME(S) AND ADDRESS(ES)

Naval Research Laboratory
Washington, DC 20375-5320

8. PERFORMING ORGANIZATION REPORT NUMBER

NRL/MR/6410--98-8190

9. SPONSORING/MONITORING AGENCY NAME(S) AND ADDRESS(ES)

Office of Naval Research
Arlington, VA 22217

10. SPONSORING/MONITORING AGENCY REPORT NUMBER

11. SUPPLEMENTARY NOTES
*Science Application International Corporation, VA
**Geo-Centers Inc., MD

12a. DISTRIBUTION/AVAILABILITY STATEMENT

Approved for public release; distribution unlimited.

12b. DISTRIBUTION CODE

13. ABSTRACT (*Maximum 200 words*)

This report is the third in a series dealing with the numerical modeling of fire suppression using water mist. In the first report, a numerical study was described for obtaining a detail understanding of the physical processes involved during the interaction of water-mist and methane-air diffusion flames. The relative contribution of the various suppression mechanisms was studied and detailed comparison with experimental results was provided. The second report described a computational study for optimizing water-mist injection characteristics for suppression of co-flow diffusion flames. The effect of droplet diameter, mist injection angle (throw angle), mist density and velocity on water-mist entrainment into the flame and flame suppression were quantified. Numerical results were presented for symmetric and asymmetric spray pattern geometries resulting from base injection and side injection nozzle orientation.

The focus of this report is on numerical modeling of methanol liquid pool fires. A mathematical model is first developed to describe the evaporation and burning of liquid methanol. Then, the complete set of unsteady, compressible Navier-Stokes equations for reactive flows are solved in the gas phase to describe the convection of the fuel gases away from the pool surface, diffusion of the gases into the surrounding air and the oxidation of the fuel molecules into product species. Heat transfer into the liquid pool and the metal container through conduction, convection and radiation are modeled by solving a modified form of the energy equation. Clausius-Clapeyron relationships are invoked to model the evaporation rate of a two-dimensional pool of pure liquid methanol. The governing equations along with appropriate boundary and interface conditions are solved using the Flux Corrected Transport algorithm. Numerical results exhibit a flame structure that compares well with experimental observations. Temperature profiles and burning rates were found to compare favorably with experimental data from single compartment and three compartment laboratory burners. The model predicts a puffing frequency of approximately 12 hz for a 1 cm diameter methanol pool in the absence of any air-co-flow. It is also observed that increasing air co-flow velocity helps in stabilizing the diffusion flame, by pushing the vortical structures away from the flame region.

14. SUBJECT TERMS		15. NUMBER OF PAGES 37
Liquid pool fires Methanol combustion Numerical modeling	Fire suppression	16. PRICE CODE

17. SECURITY CLASSIFICATION OF REPORT UNCLASSIFIED	18. SECURITY CLASSIFICATION OF THIS PAGE UNCLASSIFIED	19. SECURITY CLASSIFICATION OF ABSTRACT UNCLASSIFIED	20. LIMITATION OF ABSTRACT UL

CONTENTS

LIST OF FIGURES

Numerical Modeling of Fire Suppression using Water Mist.
3. Methanol Liquid Pool Fire Model

1. INTRODUCTION

Many common fire scenarios can be classified as pool fires. A pool fire is defined as a buoyant diffusion flame in which the fuel is configured horizontally. The fuel bed may be of an arbitrary geometry, but for simplicity, most studies consider a circular geometry characterized by a single geometrical scale, the pool diameter (D).

Water mist fire suppression of liquid pool fires has been studied for at least 50 years. Recent research in water mist technology has been driven by two events: 1) The phase out of Halon 1301 (CF_3Br) and the search for alternative technologies that preserve most of the benefits of a clean total flooding agent without the adverse environmental impact and 2) International Maritime Organization (IMO) regulations requiring retrofit of fire suppression systems on most commercial marine vessels. As a first step toward understanding the mechanisms involved in the suppression of fires, we have developed numerical models for simulating the interaction of fine water mist with methane-air gas jet diffusion flames [1], [2]. Subsequently, a study was performed to optimize various water-mist injection characteristics for maximum flame suppression [3], [4]. The effects of droplet diameter, mist injection angle (throw angle), mist density and velocity on water mist entrainment into the flame and flame suppression were quantified.

The focus of the present study is on obtaining a detailed understanding of the structure and energetics of a liquid pool fire. As opposed to earlier studies with methane-air diffusion flame, (where the fuel flow rate is held fixed at a specified value) the burning rate or the rate of evaporation of pure liquid methanol is not known a-priori. An energy equation is solved within the liquid fuel and is coupled with the gas phase through appropriate interphase conditions. This report describes a method for obtaining the burning rate of pure liquid methanol in a two-dimensional geometry. Temperature profiles obtained above a methanol liquid pool fire are compared with thermocouple temperature measurements. Once the character and structure of liquid pool fires are understood, the model will be extended to study the interaction of fine water mist with pool fires.

1.1 Literature Review

A comprehensive review of pool fires, including enclosure effects has been provided by Hall [5] and by Blinov and Khudyakov [6]. It was shown that fire hazards can be modified by ambient conditions such as the presence of an enclosure, hot surface, wind current or ventilation. These conditions were shown to play a role in governing both the detailed structure and the overall hazard of a fire. Hamins, Kashiwagi and Buch [7] have reviewed the dynamics and structure of pool fires with special regard to the flame shape, flame pulsation frequency, flame height and the

detailed flame structure. Joulain [8] has reviewed the pool fire literature with emphasis on fire safety requirements. He has addressed the influence of cross-flow, the formation and properties of soot, the heat feedback and mass burning including radiation transport and radiative energy blockage, by considering experimental approaches and some numerical modeling.

Hottel [9] has presented a semi-quantitative theory for the interpretation of the Blinov and Khudyakov [6] experiments, in which the burning rates of liquid hydrocarbons were measured over a wide range of vessel diameters. In his theory, the heat transfer from the flame to the liquid surface is divided into three terms, conductive, convective and radiative, and the burning rate is assumed to be controlled by the sum of the heat absorbed in these three forms by the liquid surface. Akita and Yumoto [10] have measured the rates of diffusive burning of liquid methanol in a special concentric vessel having three compartments as well as in a single compartment laboratory vessel. The experimental results obtained show that the burning rate is much greater at the vessel rim (next to the flame base) than near the vessel center, and that the total burning rate in the compartments of a concentric vessel is equal to that in a single vessel of the same size. A few properties of liquid fuel fires in the laminar flame region such as burning rate and the shape of the flame were measured by Nakakuki [11] using vessels of various materials and thicknesses in various ambient atmospheres. The flame was shown to contract at high ambient pressures and oxygen concentration so that the fuel and oxidant at the flame are in stoichiometric proportions. Nakakuki [12] has also performed a detailed study of the heat transfer mechanisms of liquid pool fires in small cylindrical vessels. The longitudinal temperature distribution of the vessel wall and the liquid burning rate for various materials and wall thickness were measured, and also calculated by the finite difference program. McCaffrey [13] has provided a detailed description of the distinct fluid mechanical zones observed in a buoyant diffusion flame.

Historically the modeling of pool fires has been based on the assumption that flame dynamics are similar, regardless of fire size or fuel type. Froude modeling [14] suggests that the ratio of inertia to buoyant forces is the key in simulating the fluid dynamic aspects of pool fires and that chemistry plays a secondary role. A large number of experimental, theoretical and scaling studies have investigated the coherent vortical structures which are shed by flames [14]- [19]. This phenomena has been documented for a wide range of burner diameters, heat release rates, Reynolds numbers and fuel types. The pulsing nature of the flow field propagates downstream leading to the time varying flame length. Buckmaster and Peters [15] suggested that flame pulsations were due to a modified Kelvin-Helmoltz instability. Emori and Saito [16] emphasized the importance of the Strouhal and Froude numbers in a dimensional analysis of the pulsation frequency of pool fires. The Strouhal number plotted as a function of the inverse Froude number correlates the pulsation measurements taken from the literature for 14 orders of magnitude in Froude number and covering a range of diameters from 0.007 to 50m. A buoyancy induced instability has also been observed in isothermal helium plumes. Although numerical simulations of the pulsation phenomena in non-reacting isothermal helium plumes [7] has been accomplished, the pulsing nature of buoyant fire remains to be modeled from detailed consideration of the conservation equations.

Cetegen et al. [17] have performed experiments on the periodic instability of buoyant plumes and pool fires. The periodic oscillations near the source of these flames (puffing) result in formation of large-scale flaming vortical structures at a short distance from the burner surface. These structures significantly modify the downstream flame behavior as they rise through the flame and finally burnout near the flame top. The important role of these structures on entrainment, flame

height fluctuations and radiation field from fires have been discussed in an article by Zukoski [18]. Bouhafid et al. [19] have performed a detailed mapping of the temperature, CO, CO_2 and O_2 species concentrations, and monochromatic absorption coefficient at the base region of a kerosene pool fire. Comparative analysis of the isotherm and iso-concentration patterns indicates that the buoyant flame has an intermittent character at its base, contrary to its normally attributed persistent or anchored character. The temperature field was shown to have a band of temperature maxima that approximately coincides with the luminous flame boundary.

Di Blasi [20] has reviewed the thermal degradation process of charring (wood, cellulosic materials) and non-charring materials. Gas-phase combustion processes such as ignition, flame spread and extinction are described by variable density, fully elliptic Navier-Stokes momentum, energy and chemical species mass conservation equations. Solid fuel degradation has been described by kinetic models of different complexity, varying from a simple one-step global reaction, to multi-step reaction mechanisms The single step mechanisms account only for primary solid fuel degradation, whereas semi-global reaction mechanisms account for both primary solid degradation and secondary degradation of evolved primary pyrolysis products. Using numerical techniques, Di Blasi [21] has studied the controlling mechanisms for ignition and flame spread over cellulosic fuel.

In the following sections we first develop a mathematical model for simulating the burning of methanol liquid pool fires. Although the governing equations have been written for a 2-D burner geometry, the model has also been configured for axi-symmetric pool fires. A detailed description is given of the energy equation solved in the liquid phase, the transport equations solved in the gas phase, as well as the interphase conditions that couple the gas phase with the liquid phase. The thermodynamic, radiation and kinetic models used in the analysis along with the initial and boundary conditions employed are also discussed in detail. We then discuss the numerical method used to advance the solution in a time dependent fashion and present key results for both time-dependent and steady methanol pool fires. Finally the numerical results are compared with experimental data obtained for a similar geometry.

2. MATHEMATICAL MODELS

2.1 Liquid Pool Model

Let us first consider a phenomenological description of a liquid pool fire. The energy released in the gas phase due to the exothermic chemical reactions between the fuel and the entrained oxygen heats up the methanol liquid pool. This raises the temperature of the liquid pool. At a certain temperature, the liquid pool evaporates resulting in methanol gases that convect away from the pool surface. As the pool is continuously heated, the liquid level regresses resulting in a stream of methanol gases evaporating from the pool surface. Heat is transferred through conduction and radiation from the hot combustion gases to the pool surface. This raises the temperature of the pool surface to a temperature close to the boiling point temperature of the fuel. Thermal conduction also transfers some of the energy away from the pool surface and heats up the layers of liquid methanol below the surface. As the liquid evaporates, fresh fuel is introduced through the bottom of the pool to maintain the surface of the pool at a certain level. As the fresh liquid convects upward, ultimately reaching the pool surface and then evaporating into gases, heat energy conducts downward resulting in a thermal wave propagating into the liquid pool.

We now consider the deflagration of a semi-infinite pool of pure liquid methanol. Both two-

dimensional and axi-symmetric pool geometries are considered. As in most planar flow problems, it is convenient to assume that the liquid and gas are infinite in extent and to adopt a co-ordinate system fixed to the gas-liquid interface. It is assumed that the methanol pool is stored or mounted on a platform/piston moving at a velocity equal but opposite to the local regression velocity of the fuel. As a result the location of gas-liquid interface is fixed in the laboratory frame of reference. The choice of the co-ordinate frame is for convenience only, and does not in any way constrain the regression rate of the pool. Thus in Figure 1, y is the co-ordinate normal to the pool surface; the gas liquid interface is located at $y = 0$; the liquid extends to $y = -\infty$, and the gas extends to $y = +\infty$. We are interested in computing the burning rate (mass flux rate) of the liquid fuel. Essentially, this is the rate at which the pool would move in the $+y$ direction so that the interface will remain at $y = 0$ (if we supply fresh fuel at this rate).

The burning rate of liquid methanol can be obtained as a difference between the rate of evaporation of pure liquid methanol and the rate of condensation of the gaseous products. When the gas phase and the liquid phase are in equilibrium with each other, the local gas phase vapor pressure must be equal to the Clausius-Clapeyron pressure. In the present approach, the burning rate of the methanol pool is iteratively changed until the vapor pressure equals the Clausius-Clapeyron pressure. It is assumed that the gas phase and the liquid phase are in equilibrium with each other and that the time constant associated with the equilibrium process is much smaller than all other physical processes studied in this paper.

It is assumed that the liquid only has a velocity component r_b normal to the gas-liquid interface. In other words, the horizontal velocity component (parallel to the gas liquid interface) is assumed to be zero. Experiments by Blinov and Khudyakov [6] and by Yumoto et al. [22] show that a layer of constant temperature is formed beneath the surface of the liquid fuel burning in a small glass vessel. This phenomena has been attributed to the convective motion in the liquid and cellular convection at the liquid surface (sub-surface vortex and thermal capillary flow [23]). In-spite of these observations we have chosen to neglect the horizontal motion of the fuel. We do so with the knowledge that the model will not be capable of explaining the detailed structure of the cellular patterns observed in a methanol pool and with the hope that by implicitly averaging over these structures, we will still explain properly the average temperature field, heat flux and burning rates that are observed in the experiments.

Since the velocity component parallel to the gas liquid interface is zero, the liquid convects only in the vertical direction. Furthermore, since the density of the liquid is a constant (independent of temperature), the vertical component of the velocity vector is independent of the y co-ordinate. The normal velocity component r_b (m/s) only varies in the x direction.

$$r_b = r_b(x) \tag{1}$$

With the above assumptions, one can also consider the entire liquid pool to be made up of columns that are moving at a constant velocity. Each column is of thickness equal to the grid thickness in the x direction and has its own unique velocity equal to the local regression rate or the burning rate. By using this approach, we are able to obtain a burning rate that varies along the pool surface. The average burning rate can then be obtained by integrating over the pool surface and can be compared with the experimental data available in the literature. Heat conduction in the liquid phase occurs in both the x and y direction. Assuming no chemical reaction in the liquid methanol pool, an energy conservation equation can be formulated for the pool, as follows:

$$\frac{\partial(\rho_l C_l T)}{\partial t} + \frac{\partial(\rho_l C_l T r_b)}{\partial y} = \lambda_l(\frac{\partial^2 T}{\partial x^2} + \frac{\partial^2 T}{\partial y^2}) + Q_{abs} \tag{2}$$

Here $\rho_l = 796.0 \ kg/m^3$ is the density of the liquid pool (independent of the local temperature); $C_l = 2366.45 \ J/kg/^0K$ is the thermal heat capacity; $\lambda_l = 0.195 \ J/m/s/^0K$ is the thermal conductivity of the liquid fuel; Q_{abs} is a fraction of the total radiative energy (emitted by the hot gases) absorbed at the fuel surface. The radiation model discussed later, describes the computation of the Q_{abs} in more detail (see equation 26). T is the local temperature of the liquid pool and r_b is the burning rate which varies along the pool surface and is equal to the local regression velocity of the pool. The burning rate is iteratively changed until the local vapor pressure of methanol gas above the pool surface P_{vap} is equal to the computed Clausius-Clapeyron pressure P_{cc}. The vapor pressure is related to the total pressure P as

$$P_{vap} = X_{vap}P \tag{3}$$

where X_{vap} is the mole fraction of the fuel vapor at the pool surface. The variation of the Clausius-Clapeyron pressure P_{cc} as a function of temperature T_{cc} can be computed, if the vapor pressure P_1 is known at a given temperature T_1, using the relationship

$$P_{cc} = P_1 exp\left(\frac{-\Delta H_v}{R}\left(\frac{1}{T_{cc}} - \frac{1}{T_1}\right)\right) \tag{4}$$

Here $\Delta H_v = 1.099E6 \ J/kg$ is the heat of evaporation of pure methanol liquid into vapor and R is the gas constant. The boiling point temperature $T_{boil} = 337.5^oK$ is used as T_1 and the atmospheric pressure $P_{atm} = 1.013E5 \ N/m^2$ is used as P_1.

The burning rate is iteratively changed until the local vapor pressure of methanol gas above the pool surface P_{vap} is equal to the computed Clausius-Clapeyron pressure P_{cc}. When the Clausius-Clapeyron pressure is higher than the vapor pressure, the burning rate is locally increased by an amount equal to

$$(P_{cc} - P_{vap})/P. \tag{5}$$

Conversely, when the Clausius-Clapeyron pressure is lower than the vapor pressure, the burning rate is locally decreased by the amount shown in equation 5. In order to avoid any numerical instability due to rapid changes in the burning rate, the maximum change in burning rate is restricted to 1% of its original value during any one iteration.

2.2 Gas Phase Model

As the liquid pool evaporates, a continuous stream of methanol gases convect away from the pool surface. The fuel vapor diffuses into the air flow and undergoes exothermic chemical reactions resulting in hot product gases. Detailed modeling of gas-phase reacting flows is based on a generally accepted set of time dependent coupled partial differential equations maintaining conservation of total mass, momentum, total energy and individual species density. These equations describe the convective motion of the fluid, the chemical reactions among the constituent species, and the diffusive transport processes such as thermal conduction and molecular diffusion.

A strong conservation form of the two-dimensional, unsteady, compressible Navier-Stokes equations, used to describe gas phase reactive flows systems can be written as follows.

$$\frac{\partial \rho}{\partial t} + \frac{\partial (\rho u)}{\partial x} + \frac{\partial (\rho v)}{\partial y} = 0, \tag{6}$$

$$\frac{\partial (\rho u)}{\partial t} + \frac{\partial (\rho u^2 + P)}{\partial x} + \frac{\partial (\rho u v)}{\partial y} = \frac{\partial \tau_{xx}}{\partial x} + \frac{\partial \tau_{xy}}{\partial y}, \tag{7}$$

$$\frac{\partial (\rho v)}{\partial t} + \frac{\partial (\rho u v)}{\partial x} + \frac{\partial (\rho v^2 + P)}{\partial y} = \frac{\partial \tau_{yx}}{\partial x} + \frac{\partial \tau_{yy}}{\partial y} - \rho g, \tag{8}$$

$$\frac{\partial (\rho E)}{\partial t} + \frac{\partial (\rho E + P) u}{\partial x} + \frac{\partial (\rho E + P) v}{\partial y} = \frac{\partial (\tau_{xx} u)}{\partial x} + \frac{\partial (\tau_{xy} u)}{\partial y} + \frac{\partial (\tau_{yx} v)}{\partial x} + \frac{\partial (\tau_{yy} v)}{\partial y}$$
$$- \frac{\partial q_x}{\partial x} - \frac{\partial q_y}{\partial y} - \rho g + Q_{chem} + Q_{rad}, \tag{9}$$

$$\frac{\partial \rho_k}{\partial t} + \frac{\partial (\rho_k u)}{\partial x} + \frac{\partial (\rho_k v)}{\partial y} = -\frac{\partial (\rho_k U_k)}{\partial x} - \frac{\partial (\rho_k V_k)}{\partial y} + \dot{\omega}_k, \quad k = 1, \ldots, 5 \tag{10}$$

In these equations x and y denote the independent spatial coordinate and t denotes the temporal coordinate; ρ the mass density; ρ_k the density of the k_{th} species; u and v are the x and y components of the fluid bulk velocity; P, the pressure; E, the total energy of the fluid per unit mass; g, the gravitational body force per unit mass; U_k and V_k are the x and y components of the diffusion velocity for the k_{th} species; τ_{xx}, τ_{xy}, τ_{yy} are the components of the stress tensor for newtonian fluid in rectangular coordinates; q_x and q_y are the x and y components of the heat-flux vector; ρ and ρ_k are the total gas density and individual species density. $\dot{\omega}_k$ is the rate of production of the kth species due to chemical reactions. Similarly Q_{chem} is an exothermic source term in the energy equation arising due to the oxidation of fuel molecules; Q_{rad} is the radiative heat loss term discussed later in detail.

The viscous stress terms are related to the rate of strain through the stress-strain relationship,

$$\tau_{xx} = \mu \left[\frac{4}{3} \frac{\partial u}{\partial x} - \frac{2}{3} \frac{\partial v}{\partial y} \right],$$
$$\tau_{xy} = \mu \left[\frac{\partial u}{\partial y} + \frac{\partial v}{\partial x} \right], \tag{11}$$
$$\tau_{yy} = \mu \left[\frac{4}{3} \frac{\partial v}{\partial y} - \frac{2}{3} \frac{\partial u}{\partial x} \right],$$

where, μ is the dynamic viscosity. The components of the heat flux vector contain contribution due to the heat conduction and the interdiffusion process, and can be expressed as

$$q_x = -\lambda \frac{\partial T}{\partial x} + \sum_{k=1}^{N} (h_k \rho_k U_k),$$
$$q_y = -\lambda \frac{\partial T}{\partial y} + \sum_{k=1}^{N} (h_k \rho_k V_k), \tag{12}$$

where, λ is the thermal conductivity of the fluid mixture and h_k is the enthalpy per unit mass for the k_{th} species.

The total energy per unit mass E is defined as the sum of internal energy e and the kinetic energy as follows

$$E = e + \frac{1}{2}(u^2 + v^2). \tag{13}$$

The internal energy is related to the thermodynamic pressure P through the ideal gas equation of state

$$P = R_o T \sum_{k=1}^{N} \frac{\rho_k}{W_k}, \tag{14}$$

and the caloric equation of state

$$e = \sum_{k=1}^{N} Y_k h_k - \frac{P}{\rho}, \tag{15}$$

$$h_k = \int_{T^\circ}^{T} C_{p,k} dT. \tag{16}$$

In these equations R_o is universal gas constant; W_k, the molecular weight of the kth species and $\Delta h^0_{f,k}$ are the heat of formations at the reference temperature T°.

2.3 Thermodynamics

The diffusion velocities U_k and V_k for the kth species are computed using Fick's Law, without solving the complete matrix problem associated with a multi-component system.

$$U_k = -\frac{1}{X_k} \mathcal{D}_{km} \frac{\partial X_k}{\partial x} \quad k = 1, 2, \ldots, N,$$
$$V_k = -\frac{1}{X_k} \mathcal{D}_{km} \frac{\partial X_k}{\partial y} \quad k = 1, 2, \ldots, N. \tag{17}$$

Here, $\mathcal{D}_{km}$ is the diffusion coefficient for species k diffusing into the mixture and X_k are the mole fraction of the kth species. The resulting diffusion velocities are corrected to satisfy the requirement that the diffusion velocities do not introduce any net bulk velocity to the fluid. The diffusion velocities are computed subject to the constraint equations

$$\sum_{k=1}^{N} \rho_k U_k = 0,$$
$$\sum_{k=1}^{N} \rho_k V_k = 0, \tag{18}$$

The mole fractions can be related to the mass fraction Y_k through the auxiliary relation

$$X_k = \frac{Y_k/W_k}{\sum_{k=1}^{N} Y_k/W_k}, \quad k = 1, 2, \ldots, N. \tag{19}$$

The various diffusion coefficients are obtained from detailed kinetic theory and are fitted over a suitable temperature range using a third order polynomial [24].

2.4 Kinetics

Ideally, we would like to simulate the chemical reactions by including a detailed set of elementary reactions to describe the production of the individual species and the energy release in the flame. However, the cost of computer time and memory required to track the individual species (and the elementary chemical reactions associated with the species) makes this prohibitive for problems in which parametric studies are planned. Instead, the chemical reaction and energy-release process for methane-air combustion is described phenomenologically based on a single step reaction,

$$CH_3OH + \frac{3}{2}O_2 \rightarrow CO_2 + 2H_2O, \tag{20}$$
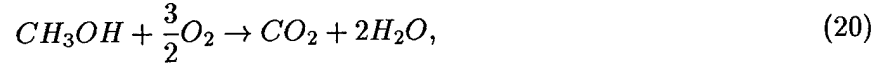
using a finite-rate, quasi-global Arrhenius expression. Westbrook et al. [25] have developed simplified reaction mechanisms for the oxidation of hydrocarbons using a laminar flame model and prescribed an overall rate of consumption of methanol as

$$\frac{d[CH_3OH]}{dt} = -1.0E11 exp(-15000/RT)[CH_3OH]^{0.25}[O_2]^{1.5}. \tag{21}$$

The above expression is used to compute the depletion of methanol. The stoichiometric coefficients provided in Eqn. (20) is then used to compute the corresponding changes in the concentration of oxygen, carbon dioxide, water vapor and nitrogen. The heat release term Q_{chem} appearing in the energy Eqn. (10) is determined from

$$Q_{chem} = -\Delta H_c \frac{d[CH_3OH]}{dt}, \tag{22}$$

where $\Delta H_c = 22.0E6 \ J/kg$ is the heat of combustion for the single step global chemical reaction per unit mass of fuel. The heat of combustion is computed using the stoichiometric coefficients and the heat of formation of the various species as follows,

$$\Delta H_c = \sum_{k=1}^{N} (\nu_k'' - \nu_k')\Delta h_{f,k}^0, \tag{23}$$

where, ν_k' and ν_k'' are the stoichiometric coefficients of the kth species as a reactant and product respectively and $\Delta h_{f,k}^0$ are the heat of formation of the kth species. The reaction rate equations involving the Arrhenius terms are solved using an implicit trapezoidal scheme with time step splitting over the largest fluid dynamic time step.

2.5 Radiation Model

It has long been recognized [26]- [29] that radiation is the dominant mode of heat transfer in fires of very large scale; whereas convection (or conduction) is the dominant mode in fires of very small scale. The general success of predicting small scale laminar burning as convection dominated has led to a prolonged neglect of radiation by some fire researchers. However in recent years, detailed heat transfer measurements have demonstrated that radiative heat transfer from flames to fuel surfaces can typically exceed free convective heat transfer for characteristic flame lengths greater than $0.2m$ [26].

Since methanol (CH_3OH) is a relatively low sooting fuel, the optically thin assumption is used in the radiation transport sub-model,

$$Q_{rad} = 4a_{overall}\sigma(T^4 - T_\infty^4),\tag{24}$$

where $\sigma = 5.67\text{E-}8\ W/m^2/K^4$ is the Stefan-Boltzmann constant; T is the local temperature of the gas phase and T_∞ is the ambient temperature. The overall absorption coefficient ($a_{overall}$) for CO_2 and H_2O are derived using a temperature dependent polynomial relation obtained from Hubbard and Tien [30].

In order to compute the radiative heat transfer from the luminous flame and the hot product gases to the liquid fuel, configuration factors ϕ are computed. The configuration factors account for the fraction of radiative energy that is absorbed by the methanol fuel to the total radiative energy emitted by the hot gas. The configuration factor ϕ between any gas-phase co-ordinate point (x_i, y_j) and a liquid surface co-ordinate point (xs_i, ys_j) is expressed as follows

$$\phi = \frac{(xs_{i+1} - xs_i)}{2.0\pi\sqrt{((x_i - xs_i)^2 + (y_j - ys_j)^2)}}.\tag{25}$$

Thus the energy absorbed at the fuel surface Q_{abs} is a fraction of the total energy radiated Q_{rad} from any location in the gas phase and is expressed as follows

$$Q_{abs} = \phi\frac{(x_{i+1} - x_i)(y_{j+1} - y_j)}{(xs_{i+1} - xs_i)(ys_{j+1} - ys_j)}Q_{rad}.\tag{26}$$

Eqn. (26) also accounts for the differences in the cell sizes that are radiating and absorbing the energy. Note that subscripts $i+1$ and $j+1$ refer to adjacent node points. A Beer's law model is further used to describe the reduction in beam irradiance brought about by absorption in the liquid phase. An absorption coefficient $\alpha = 1/(4\mu m)$ is assumed for the methanol liquid. The energy input at any node in the liquid phase is obtained by subtracting the beam irradiance leaving the cell from that at the input to the cell.

2.6 Boundary and Interphase Conditions

A specific solution of the reactive flow equations is determined by the initial conditions and the boundary conditions that describe the geometry of the system and exchange of mass, momentum and energy occurring between the system and the rest of the physical world. Fresh methanol liquid enters through the inflow boundary of the methanol pool at a fixed temperature equal to the ambient temperature

$$T(inflow\ boundary) = T_0 = 298^0K.\tag{27}$$

As discussed earlier, the velocity component parallel to the gas-liquid interface is zero, and the liquid convects only in the vertical direction. The normal velocity component r_b varies only in the x direction. The velocity r_b with which fresh methanol flows into the pool is specified at the inflow boundary. During the course of the simulation this burning rate is iteratively changed until the local vapor pressure is equal to the computed Clausius-Clapeyron pressure. Air enters the computational domain through the air channel inflow boundary. The total density, u and v momentum, temperature T, and the various species densities are prescribed at the inflow boundary.

At the outflow boundary, the normal gradients of total density, momentum and all species densities was assumed to be zero,

$$\frac{\partial(\rho)}{\partial x} = \frac{\partial(\rho u)}{\partial x} = \frac{\partial(\rho v)}{\partial x} = \frac{\partial(\rho_k)}{\partial x} = \frac{\partial(T)}{\partial x} = 0. \tag{28}$$

The pressure at large distances (64× thickness of fuel container) from the burner surface is assumed to be equal to the ambient pressure.

A symmetric boundary condition was employed at the center line of the computational domain by use of anti-symmetric reflection of the gas phase tangential velocity v , and symmetric reflection of all other variables. A slip wall boundary condition is employed at the lateral boundary by assuming that the flux of all transported properties across the wall is zero. For the methanol liquid pool, symmetric boundary condition was employed at the center line of the computational domain by use of symmetric reflection of temperature T. The steel container is assumed to loose heat to the surrounding air through conduction. The temperature of this surrounding air is always set at a room temperature of $298^0 K$.

In addition to specifying the boundary conditions, one needs to specify specialized interface conditions that account for the transition from the liquid phase to the gas phase. In order to specify the interface conditions for the gas phase a ghost layer is introduced just above the gas-liquid interface as shown in Figure 2. Here l_1 refers to grid line in the liquid layer lying adjacent and parallel to the gas liquid interface. The grid lines l_2 and l_3 lie below the gas-liquid interface. Similarly grid line g_1 is for gas phase grid line lying above the gas-liquid interface. At these ghost cells, the values for the various gas flow variables are specified. The introduction of the ghost cells provide an easy way to couple the gas phase with the liquid phase. Mass conservation is satisfied at the ghost cell by algebraic relations that relate the ghost cell values to the adjacent grid point in the liquid layer $(l1)$.

$$(\rho u)_{ghost} = 0, \tag{29}$$

$$(\rho v)_{ghost} = \rho_l r_b. \tag{30}$$

Similarly, energy conservation is maintained by accounting for the heat of sublimation associated with the evaporation process as follows,

$$(\rho E)_{ghost} = \rho_{ghost}(C_l T_{l1} - \Delta H_v) + 0.5 * \frac{(\rho_l r_b)^2}{\rho_{ghost}}, \tag{31}$$

where $\Delta H_v = 1.099 E6 J/kg$ is the heat of sublimation associated with the evaporation process of liquid methanol (CH_3OH).

It is assumed that the pressure gradient at the liquid surface are zero. Therefore

$$P_{ghost} = P_{g1} \tag{32}$$

The temperature of the ghost layer is equal to the temperature of the adjacent liquid layer $T_{ghost} = T_{l1}$. The total density and the various species densities at the ghost layer can then be computed as follows

$$\rho_{ghost} = \frac{P_{ghost}}{T_{ghost} * R}, \tag{33}$$

$$(\rho_k)_{ghost} = \rho_{ghost} \quad k = CH_3OH, \tag{34}$$

$$= 0 \qquad k \neq CH_3OH. \tag{35}$$

For the liquid layer, ghost cells are introduced at the grid point $g1$ as shown in Figure 2. Energy conservation is maintained by setting $T_{ghost} = T_{g1}$ for providing interface conditions for the liquid layer.

To account for the heat conduction from the gas phase to the liquid phase, the energy equation 2 solved at the gas-liquid interface (grid point l1) is modified as follows

$$\frac{\partial(\rho_l C_l T)}{\partial t} + \frac{\partial(\rho_l C_l T r_b)}{\partial y} = \lambda_l \frac{\partial^2 T}{\partial x^2} + \frac{(\lambda_g \frac{\partial T}{\partial y}|_{l1} - \lambda_l \frac{\partial T}{\partial y}|_{l2})}{y_{l1} - y_{l2}} + Q_{abs}. \tag{36}$$

The heat conduction terms are differenced as follows

$$\frac{\partial T}{\partial y}|_{l1} = (T_{g1} - T_{l1})/(y_{g1} - y_{l1}) \tag{37}$$

$$\frac{\partial T}{\partial y}|_{l2} = (T_{l1} - T_{l2})/(y_{l1} - y_{l2}) \tag{38}$$

Similarly to account for the heat losses from the liquid pool to the surrounding air, the energy equation 2 is written to account for the different heat capacities in the air and liquid methanol. It is assumed that the temperature of the air is maintained at a room temperature of $298^{\circ}K$.

2.7 Initial conditions

The computations are initiated by setting the liquid pool temperature to be equal to the ambient temperature. An average burning rate as obtained from experimental results (or an estimate) is used as the local burning rate at each point over the entire pool surface. The initial conditions for the gas phase assume that there is a column of pure methanol gas rising from the pool surface. The rest of the computational domain consists of air moving at a velocity equal to the air inlet velocity.

3. NUMERICAL ALGORITHMS

The governing equations are rewritten in terms of finite-volume approximations on an Eulerian mesh and solved numerically for specific boundary and initial conditions. A complete solution to these governing equations require solving the terms for each of the individual processes, as well as accounting for the interaction among the processes. The solution approach consists of separate algorithms for each of the individual processes, which are then coupled together by the method of time-step splitting [31]. The algorithms for convection, thermal conduction, molecular diffusion, viscosity and the coupling of the individual processes have been previously discussed in detail [32].

The fluid convection is solved with a high-order implicit algorithm, Barely Implicit Correction to the Flux-Corrected Transport (BIC-FCT), that was developed to solve the convection equations for low-velocity flows [33]. The Flux-Corrected Transport (FCT) algorithm itself is an explicit, finite-difference algorithm that is constructed to have fourth-order phase accuracy [34]. Through a two-step predictor-corrector procedure, FCT ensures that all conserved quantities remain monotone and positive. The FCT procedure is to first modify the properties of a high-order algorithm by adding diffusion during a convection step and then to subtract out the diffusion in an antidiffusion phase. In addition, fluxes are limited to ensure that no new unphysical maxima or minima are added

during the convection process. However, because FCT is an explicit algorithm, the numerical time-step required for accuracy and stability is limited by the velocity of sound according to the CFL condition. To filter out the sound waves from the convection equations and therefore remove the sound-speed (Courant) limitation on the time-step, the convection equations are usually solved implicitly. The BIC-FCT algorithm was developed so that the time step is limited by the fluid velocity and not the sound speed. This implementation is particularly useful for slowly evolving flows because one BIC-FCT time-step requires the same amount of computer time as one regular FCT explicit time step, but the size of the timestep might be a factor of 50-100 times greater.

The computational domain in the gas phase consists of a stretched 120×128 grid, concentrated near the contact point of the fuel and the oxidizer. The overall dimensions of the gas phase computational domain are 9.5 cm in the x direction and 64.0 cm in the y direction. The methanol pool has a thickness of 1.0 cm, and a typical flame is 2.0 cm to 3.0cm long. The smallest grid cell is 60 μm in the x direction and 66 μm in the y direction. The computational domain in the liquid pool again consists of a stretched cartesian 32×96 grid, concentrated near the outer edge of the pool. The smallest grid cell is 60 μm in the x direction and 2 μm in the y direction. In the x direction, the grid is essentially extended from the gas phase into the liquid phase. In the y direction, the grid is concentrated close to the liquid pool surface in order to capture the structure of the thermal wave. The grid stretches gradually as one moves away from the pool surface. Numerical simulations were performed by halving the grid size to check for accuracy and consistency of the algorithms. The algorithms have been optimized for efficient performance on vector machines. Typical computational time on a C-90 single processor machine was approximately 10 hours to reach a steady state solution.

4. RESULTS AND DISCUSSION

Figure 1 is a schematic diagram of a two-dimensional methanol pool burner geometry. The figure also shows some of the important physical processes involved in the evaporation and combustion of liquid methanol. The fluid dynamic equations, describing the gas and the liquid phase, presented earlier were solved using the numerical methodology briefly discussed above, to study two-dimensional liquid methanol pool fires stabilized above a Wolfhard-Parker diffusion flame burner. The diffusion flame stabilized above the methanol pool heats up the liquid due to conductive, convective and radiative heat transfer. Heat is also transferred to the liquid through the metal container. This raises the temperature of the liquid to a temperature close to the boiling point. As the methanol pool evaporates it provides a continuous supply of methanol gas which subsequently undergoes combustion resulting in product gases. As the pool evaporates fresh fuel is introduced through the bottom in order to maintain the liquid pool surface level with the metal container. Experimentally, a self-leveling mechanism is utilized to maintain the pool surface at a certain level. This mechanism ensures that the height of the lip above the pool surface is held fixed during the entire experiment. For the present study it is assumed that the liquid is flush with the metal container (the height of the lip is assumed to be zero).

4.1 Unsteady Pulsating Pool Fires

Numerical simulations have been performed to study the various physical processes involved during burning of a methanol pool, with and without a co-flowing air jet. Figure 3 shows the typical temperature (^0K) and heat release rate ($J/m^3/s$) contours above a methanol liquid pool

fire, with an air co-flow velocity of 10.0 cm/s. The heat release rate profile indicates the region of rapid exothermic chemical activity. This profile also identifies the location of the flame sheet where the fuel and the oxidizer species come together in stoichiometric proportions, react exothermically and produce product species. The heat release rate contours indicate the presence of a thin flame sheet which closes above the fuel duct. The vorticity contours shown in Figure 4 clearly show the presence of coherent vortical structures which are shed by the fire periodically. This phenomena has been documented for a wide range of burner diameters, heat release rates, Reynolds number and fuel types. The vortical structures and their shedding frequency influence the rate of air entrainment into the fire. The pulsing nature of the flow field propagates downstream leading to a time varying flame length. The average height of the flame is roughly 3.5 cm and the maximum flame temperature is $1840K$ which agrees well with experimental data.

Figure 5 shows contour plots of gaseous methanol (CH_3OH) and oxygen (O_2) density (kg/m^3) above the burner surface. Due to the oxygen rich environments for which these simulations were performed, methanol gas is completely consumed. The unused oxygen is entrained along with the hot product gases and flows out of the computational domain. Figure 6 shows density distributions of the product species, carbon-dioxide (CO_2) and water vapor (H_2O). Figure 7 shows the velocity vectors and streamline pattern. The velocity vectors have been color coded with red showing the highest gas velocity and blue showing the lowest gas velocity. The direction of the arrows shows the direction of the velocity vector. The particle path lines clearly shows the entrainment of the oxidizer into the diffusion flame. Both the streamlines and velocity vectors bend into the flame due to the entrainment of air into the diffusion flame. Velocity vectors in Figure 7 show that a symmetrical vortex is formed along the liquid surface in the center of the vessel, and that ambient air penetrates deep into the flame at the vessel rim. Apparently these vortices, as well as the large entrained air zone, are characteristic of diffusive burning of liquid fuels in small vessels since, similar features have also been observed by Akita and Yumoto [10] in their flame photographs with particle tracks and by Hirst and Sutton [35].

Figure 8 shows temperature contours at various time levels (0.019, 0.039, 0.058, 0.076 and 0.093 s) showing the pulsating nature of the diffusion flame. The gross structure of a buoyant fire can be described in terms of three regions; a fuel rich core know as the persistent zone, an intermittent region with a time varying visible flame tip and a downstream plume region. The fuel rich core (up to a height of 1.0 cm above the burner surface) is the region just above the fuel surface where little oxygen has penetrated. This region is relatively cool and rich in fuel. Large scale vortices roll into the fire, entrain air, and define the boundaries of the fuel rich core. Above the fuel rich core is the intermittent region ($1.0 - 4.0 \, cm$) where air is convected radially into the fire. Heat is released as the fuel reacts with the entrained air, yielding combustion products. In the fire plume ($> 4.0 \, cm$), the rate of chemical reactions decrease exponentially as the temperature drops and more cold air is entrained. These observations qualitatively compare with the experimental results from McCaffrey [13].

In general the flame shape changes with time through a pulsation cycle. The puffing mechanism involves acceleration of buoyant plume gas in the stagnant surroundings resulting in formation of toroidal vortical structures within one burner diameter above its surface, accumulation of buoyant gas inside the flame envelope and its buoyant acceleration to form the next vortical structure. The average shedding frequency based on the temperature contours (Figure 8) and vorticity contours (Figure 4) was found to be approximately 12 Hz. Cetegen et. al [17] has reported puffing frequencies

as a function of burner diameter for various fuels and over a wide range of burner diameters. It was found that the puffing frequency for buoyant plumes and flames scales as $D^{-1/2}$ and that this scaling is related to the convection speed of the toroidal vortices. The puffing frequency obtained from our numerical simulations compares favorably with data compiled by Cetegen et al. [17] and reported in references [7], [36] - [38].

As the flame pulsates periodically and sheds the vortices, the heat transfer to the liquid pool also changes and this affects the average burning rate of the pool. The variation of average burning rate as a function of time has been shown for air co-flow velocities of 10 cm/s and 2 cm/s in Figure 9. An average burning rate of 1.6E-5 m/s and 1.35E-5 m/s was obtained for air co-flow velocity of 10 cm/s and 2 cm/s respectively. As the co-flow velocity increases to 40 cm/s the average burning velocity also increases to 2.4E-5 m/s. As the air co-flow velocity increases we observe that the unsteadiness in the average burning rate reduces. This is due to the fact that as the air co-flow velocity increases the vortices that entrain air into the flame are convected downstream and are located further away from the burner surface. We also observe that the flame height increases as the air co-flow velocity increases.

4.2 Steady Pool Fires

Experimentally it is very difficult to make temperature measurements of a pulsating pool fire. In order to stabilize the pool fire, the air co-flow velocity was increased to 20 cm/s and 40 cm/s. As discussed above, the air co-flow stabilizes the diffusion flame. The vortical structures are now located very far from the burner surface. For the higher air co-flow velocities thermocouple temperature measurements can be made for the temperature profiles across a methanol pool fire. Figure 10 shows the temperature (K) and heat release rate contours ($J/m^3/s$) above a methanol pool fire stabilized by a co-flowing air jet (20 cm/s). The numerically computed flame height is approximately 18 mm long. The temperature contours and the heat release rate contours appear to be similar to those that are observed for any hydrocarbon diffusion flame stabilized above a Wolfhard Parker diffusion flame burner. Numerically computed temperature contours were compared with experimental measurements obtained over a similar geometry.

4.3 Comparison with Experimental Results

The key component of the experimental setup is a modified Wolfhard-Parker burner. A schematic diagram of the burner geometry was given in Figure 1 of Reference [2]. The burner slot is 7.5 cm long, 1.0 cm wide and 15.0 cm deep. It has two identical oxidizer channels 8.2 cm long, 3.5 cm wide and 15.0 cm deep on each side. In the current experiments the average exit velocity of the air is 18.1 cm/s. Pure liquid methanol is placed in the fuel vessel. The level of methanol is maintained at a fixed level flush with the metal container. This is accomplished by a self leveling mechanism. A quartz glass shield, 47 cm long and 27 cm high sits on the burner on either side to protect the flame from any external disturbances. The flame temperature is measured with a 50 μm diameter fine platinum/platinum - 13% - rhodium thermocouple which is computer controlled by a Newport 3D positioning instrument.

Figure 11 shows comparison between numerically obtained temperature profiles and experimentally measured thermocouple data. Comparison was made at six different heights above the burner surface. At each height above the burner surface it was found that the numerically computed

temperature profiles are in good agreement with the experimental measurements. Experimentally the methanol pool fire height is approximately 15 *mm* long and this is exhibited by the absence of the bi-modal temperature profile at a height of 15 *mm* above the burner surface. Numerical simulations indicate a flame height of about 18 *mm* (See Figure 10). Inspite of this difference, the comparison between numerical and experimental results is deemed satisfactory, considering all the simplifying assumptions made in the model and uncertainties in thermocouple measurements.

As discussed in the section dealing with the liquid pool model, an energy equation is solved to obtain the temperature distribution in the methanol liquid pool. Figure 12 shows the temperature contours within the liquid pool. The temperature contours clearly show the structure of the thermal wave propagating into the liquid pool. The variation of pool surface temperature as a function of distance along the pool surface has also been shown in Figure 12. It is observed that the pool surface temperature is very close but lower than the boiling point temperature of pure liquid methanol ($T_{boil} = 337.5$ K). The pool surface temperature is highest in the center of the pool and falls down to $322.5K$ at the pool edge. This reduction in pool temperature is due to heat losses to the surrounding air and the metal container. Another reason for the lower temperature at the pool edge is that the local burning rate is very high at the pool edges. As a result fresh methanol fuel at room temperature is convecting towards the pool surface at a higher rate which in turn leaves very little time for thermal heating of the fuel.

4.4 Burning Rates

The local burning rate (or the rate of evaporation) as a function of distance along the pool surface has been shown in Figure 13 for two different air co-flow velocities of 40 *cm/s* and 20 *cm/s*. We observe that the burning rate is very high at the pool edges and is smallest at the pool center. The burning rate at the pool edge is dominated by conductive heat transfer whereas that at the pool center is dominated by radiative heat transfer. The local burning rate can be integrated over the entire pool surface to give the total burning rate. The average burning rate shown in Figure 13 is obtained by dividing the total burning rate by the pool area. We obtain an average burning rate of 2.4E-5 *m/s* and 1.7E-5 *m/s* for air co-flow velocities of 40 *cm/s* and 20 *cm/s* respectively. The experiments indicate an average burning rate of 2.7E-5 *m/s*. It should be noted that numerical simulations indicate a local burning velocity at the pool edges significantly higher than the average burning velocity. This implies that the methanol gases evaporating from the pool edges are flowing at a speed 25-50 times higher than those originating at the center of the pool.

Numerical simulations were also performed for axi-symmetric pool fire with zero co-flow velocity and results were compared with experimental data from Akita and Yumoto [10]. Numerical simulations for axi-symmetric pool fires show an average burning rate of 3.4E-5 *m/s*, whereas experimental results [10] show an average burning rate of 5.0E-5 *m/s*. Akita and Yumoto [10] have measured burning rates of liquid methanol in special concentric vessels having three compartments. They observe that the burning rate is highest in the outermost compartment and smallest in the innermost compartment. This observation is again in favorable agreement with numerical results shown in Figure 13.

As discussed earlier, the burning rate is iteratively changed until the local vapor pressure of methanol gas above the pool surface is equal to the computed Clausius-Clapeyron pressure P_{cc}. Figure 14 shows the comparison between the vapor pressure and the computed Clausius-Clapeyron

pressure as a function of distance along the pool surface. At the center of the pool, the gas mixture contains a very high mole fraction of methanol gas resulting in higher vapor pressure. At the pool edges, the gas mixture is diluted by diffusion of air into the fuel. This reduces the vapor pressure. Figure 14 shows that under steady state conditions the vapor pressure and the Clausius-Clapeyron pressure are almost equal to each other showing that methanol gas and liquid are in local equilibrium with each other.

5. WORK IN PROGRESS

The mathematical models that were discussed in this report for studying the evaporation and burning of liquid methanol are being combined with a water-mist model to study the suppression of fires using "Class 1" droplet sprays. The water-mist model [1], [2] described using an Eulerian formulation is coupled with the gas phase through the source terms. In this model, the droplet properties are treated as if they are continuous in the domain as the gas properties.

The following additional studies are being conducted to obtain a detailed understanding of the physical processes involved during the interaction of water-mist and liquid methanol pool fires.

- The effect of various water-mist injection characteristics (base injection, side injection or top injection) on overall flame suppression.
- The changes in average burning rate as a function of water-mist injection density.
- The effect of symmetric and asymmetric injection on overall flame suppression.
- The relative importance of the various flame suppression mechanisms.
- The effect of droplet diameter, spray injection density and velocity on water-mist entrainment into the flame.

6. ACKNOWLEDGEMENT

7. REFERENCES

1. Prasad, K., Li, C., Kailasanath, K., Ndubizu, C., Gopal, R. and Tatem, P.A., *Numerical Modeling of Water Mist Suppression of Methane-Air Diffusion Flame*, Comb. Sci. & Tech., V. 132, 1-6, p-325 (1998).

2. Prasad, K., Li, C., Kailasanath, K., Ndubizu, C., Gopal, R. and Tatem, P.A.,*Numerical Modeling of Fire Suppression Using Water Mist. 1. Gaseous Methane-Air Diffusion Flame*,Naval Research Laboratory Report, NRL/MR/6410-98-8102 (1998).

3. Prasad, K., Li, C. and Kailasanath, K., *Numerical Modeling of Fire Suppression Using Water Mist. 2. An Optimization Study on Jet Diffusion Flames*, Naval Research Laboratory Report, NRL/MR/6410-98-8159 (1998).

4. Prasad, K., Li, C. and Kailasanath, K., *Optimizing Water-mist Injection Characteristics for Suppression of Co-flow Diffusion Flames*, Twenty-seventh Symposium (International) on Combustion, (1998).

5. Hall, A. R., Oxidation and Combustion Review, 6, 169 (1973).

6. Blinov, V.I., and Khudyakov, G.N., *Diffusion Burning of Liquid*, U.S. Army Engineering Research Development Laboratories, T-1490 a-c, ASTIA AD 296, 762, p.125.

7. Hamins, A., Kashiwagi, T. and Buch, R., *Characteristics of Pool Fire Burning*, Fire Resistance of Industrial Fluids, ASTM STP 1284, George E. Totten and Jurgen Reichel, Eds. American Society for Testing and Materials, Philadelphia, (1995).

8. Joulain, P., *The Behavior of Pool Fires : State of the Art and New Insights*, Twenty-seventh Symposium (International) on Combustion, (1998).

9. Hottel, H. C., Fire Research Abstract Reviews, 1, 41, (1959).

10. Akita, K. and Yumoto, T., *Heat Transfer in Small Pools and Rates of Burning of Liquid Methanol*, Tenth Symposium (International) on Combustion, pp.943-948, (1965).

11. Nakakuki, A., *Liquid fuel Fires in the Laminar Flame Region*, Combustion and Flame, 23, 337-346 (1974).

12. Nakakuki, A., *Heat Transfer in Small Scale Pool Fires*, Combustion and Flame, 96:311-324 (1994).

13. McCaffrey, B. J., Center for Fire Research, NBSIR 79:1910 (1979).

14. Orloff, L. and De Ris, J., *Froude Modeling of Pool Fires*, Nineteenth Symposium (International) on Combustion, The Combustion Institute, pp. 885-895, (1982).

15. Buckmaster J. and Peters, N., Twenty-First Symp. (International) on Combustion, p. 677, (1988).

16. Emori, R. I. and Saito, K., Combustion Science and Technology, 31, 217, (1983).

17. Cetegen, B. M. and Ahmed, T.A., *Experiments on the Periodic Instability of Buoyant Plumes and Pool Fires*, Combustion and Flame, 93: 157-184 (1993).

18. Zukoski, E. E., Proceedings of the First International Symposium on Fire Safety Science, (1985).

19. Bouhafid, A., Vantelon J. P., Joulain, P. and Fernandez-Pello, A. C., *On the Flame Structure at the Base of a Pool Fire*, Twenty-Second Symposium (International) on Combustion, The Combustion Institute, pp.1291-1298, (1988).

20. Di Blasi, C., *Modeling and Simulation of Combustion Processes of Charring and Non-charring Solid Fuels*, Prog. Energy Combust. Sci., Vol. 19, pp. 71-104, (1993).

21. Di Blasi, C. and Wichman, I. S., *Effects of Solid-Phase Properties on Flames Spreading over Composite Materials*, Combustion and Flame, Vol. 102, 3, pp. 229, (1995).

22. Yumoto, T., Takahashi A. and Handa T., *Combustion Behavior of Liquid Fuel in a Small Vessel: Effect of Convection Motion in the Liquid on Burning Rate of Hexane in the Early Stage of Combustion*, Combustion and Flame, 30, p. 33-43, (1977).

23. Miller, F. J. and Ross, H. D. " Smoke Visualization of the Gas-Phase flow During Flame Spread Across a Liquid Pool" Twenty-seventh Symposium (International) on Combustion, (1998).

24. Kailasanath, K., Oran, E.S. and Boris, J.P., NRL Memorandum Report, 4910, (1982).

25. Westbrook, C. K. and Dryer, F. L., Comb. Sci. & Tech., Vol. 27, pp. 31-43, (1981).

26. De Ris, J., Seventeenth Symposium (International) on Combustion, p. 1003, The Combustion Institute, (1979).

27. Orloff, L., *Simplified Radiation Modeling of Pool Fires*, Eighteenth Symposium (International) on Combustion, The Combustion Institute, p. 549, (1981).

28. Fischer, S. J., Hardouin-Durparc, B. and Grosshandler, W. L., *The Strucuture and Radiation of an Ethanol Pool Fire*, Combustion and Flame, 70:291-306 (1987).

29. Xhang, X. L., Vantelon, J.P. and Joulain, P., *Thermal Radiation from a Small-Scale Pool Fire: Influence of Externally Applied Radiation*, Combustion and Flame, 92:71-84 (1993).

30. Hubbard, G. L. and Tien C. L., *Infrared Mean Absorption Coefficients of Luminous Flames and Smoke*, Journal of Heat Transfer, Vol. 100, p. 235, (1978).

31. Oran E.S. and Boris, J. P., *Numerical Simulation of Reactive Flow*, Elsevier Publication, 1987.

32. Ellzey, J.L., Laskey, K.J., Oran, E.S and Brun, T.A., *FLIC- A Detailed Two-Dimensional Flame Model*, NRL Memorandum Report, 6555, 1989.

33. Patnaik, G., Laskey, K.J., Kailasanath, K., Oran, E.S. and Brun, T.A., *FLIC - A Detailed, Two-Dimensional Flame Model*, NRL Memorandum Report, 6555, (1989).

34. Boris, J.P., and Book, D.L., *Flux Corrected Transport I. SHASTA, A Fluid Transport Algorithm That Works*, Journal of Computational Physics, 11 (1) pp.38-69, (1973).

35. Hirst, R. and Sutton, D., Combustion and Flame, 5, 319, (1961).

36. Schoenbucher, A., Arnold, B., Banhardt, V., Bieller, V., Kasper, H., Kaufmann, M., Lucas, R., and Sciess, N., Twenty-First Symposium (International) on Combustion, The Combustion Institute, Pittsburgh, p.83, (1986).

37. Weckman, E. J. and Sobiesiak, A., Twenty-Second Symposium (International) on Combustion, The Combustion Institute, p.1299, (1988).

38. Brotz, W., Schoenbucher, A., Banhardt, V. and Sciess, N., Phys. Chem, 87:99 (1983).
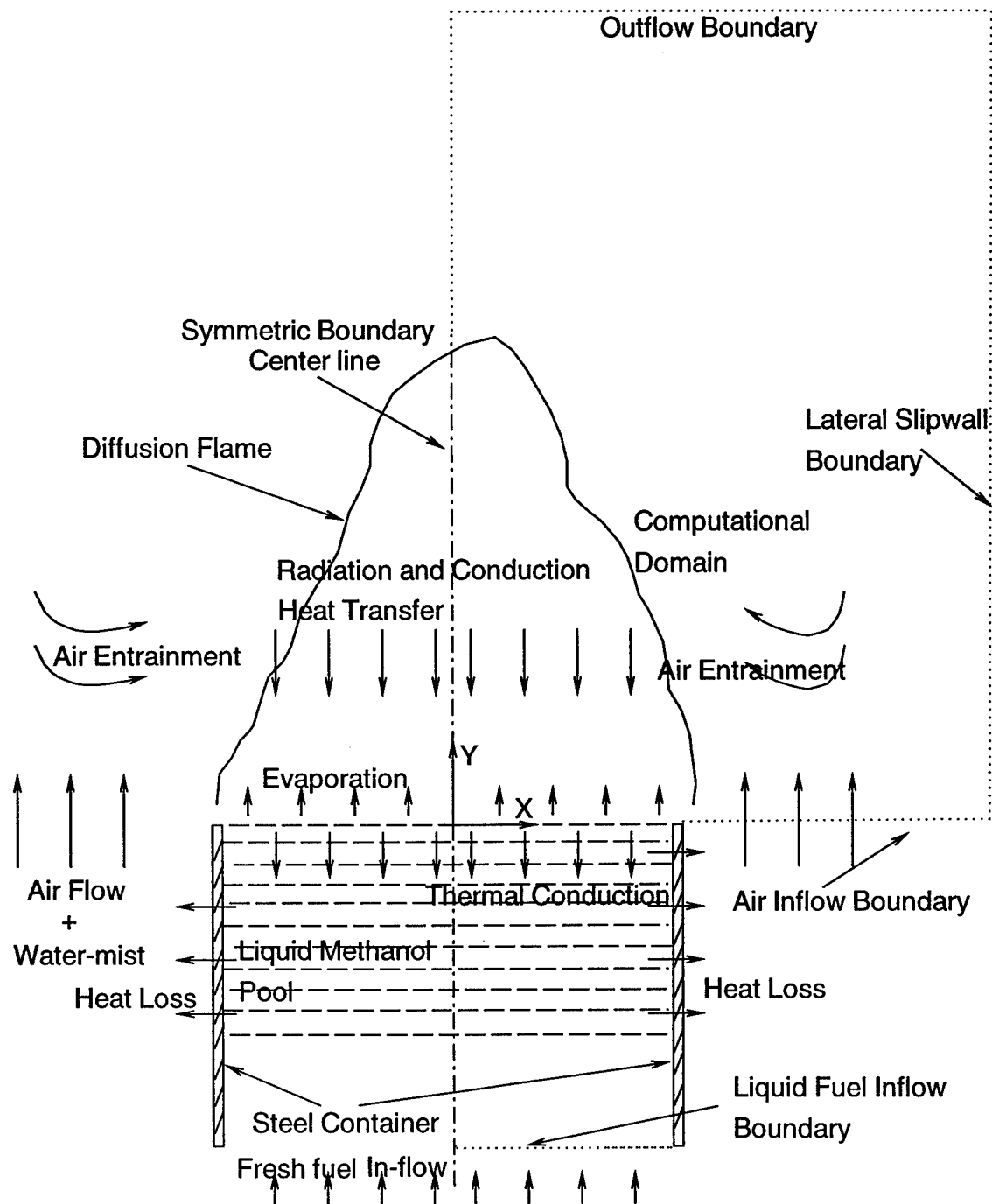
Fig. 1. Schematic diagram of a methanol liquid pool fire burner geometry. The gas phase and the liquid phase computational domain in which the solutions are desired have been shown along with some of the physical processes involved during the evaporation of liquid methanol.
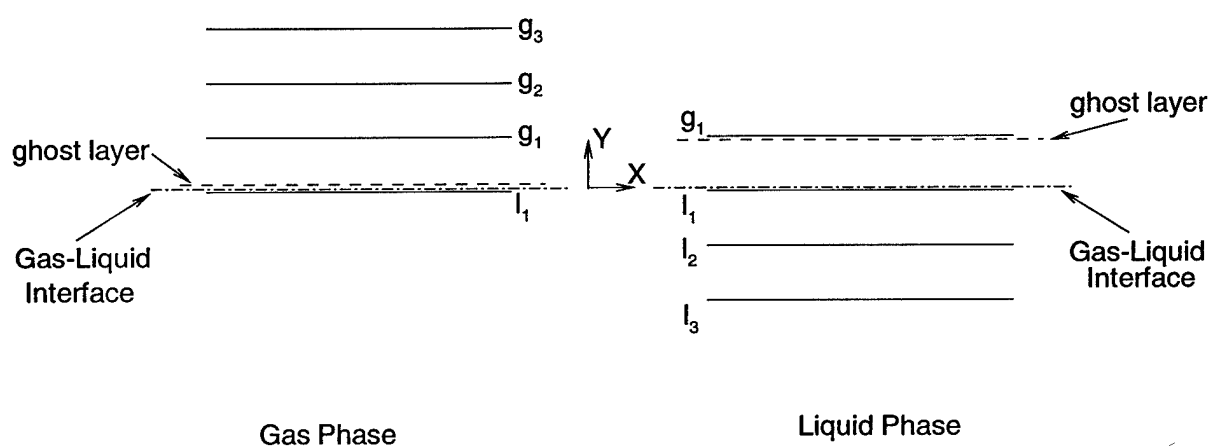
Fig. 2. Location of the gas-liquid interface and the ghost cells in relation to the grid and the coordinate system.
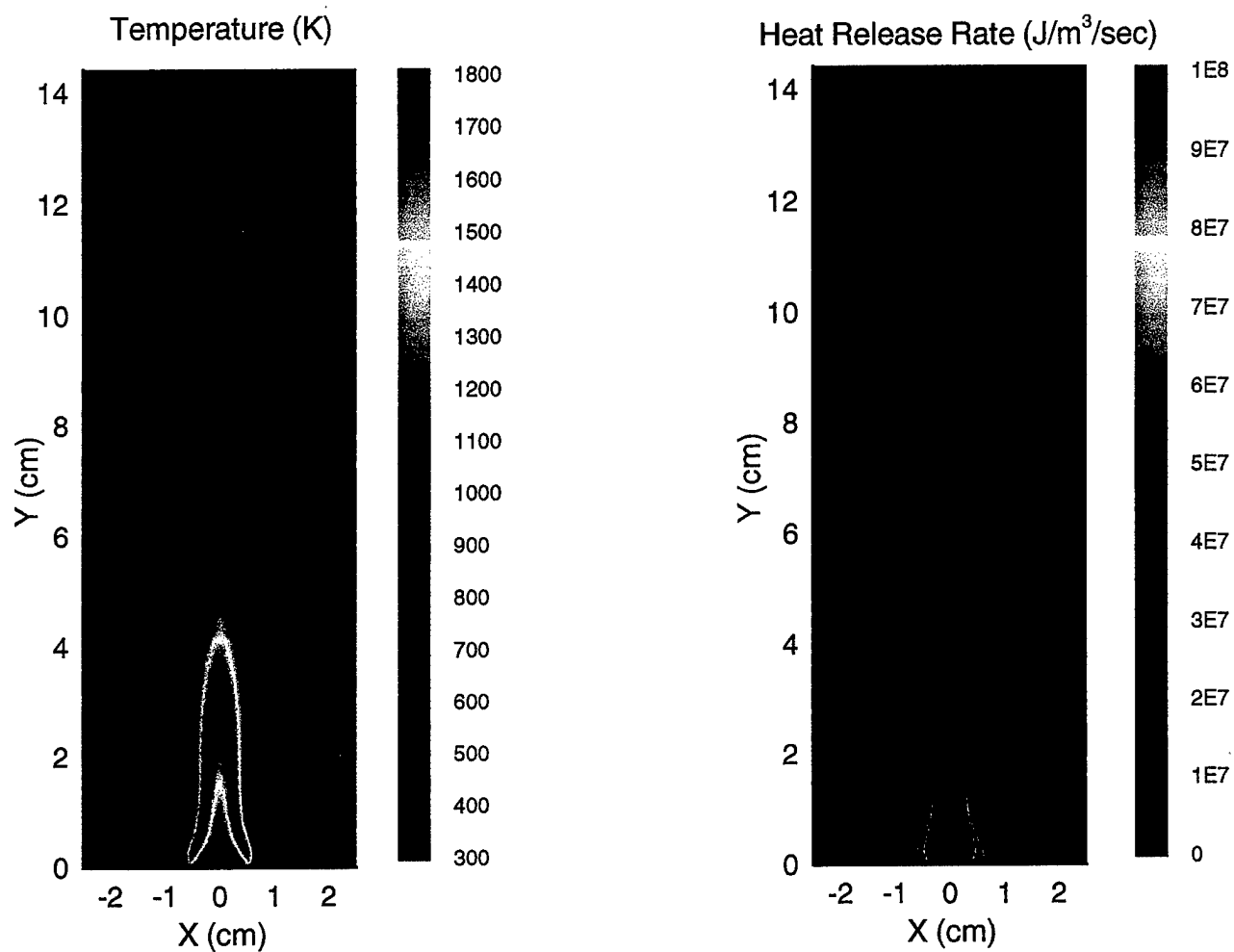
Fig. 3. Typical temperature (K) and heat release rate $(J/m^3/s)$ contours above a methanol liquid pool fire illustrating the puffing nature of the diffusion flame.
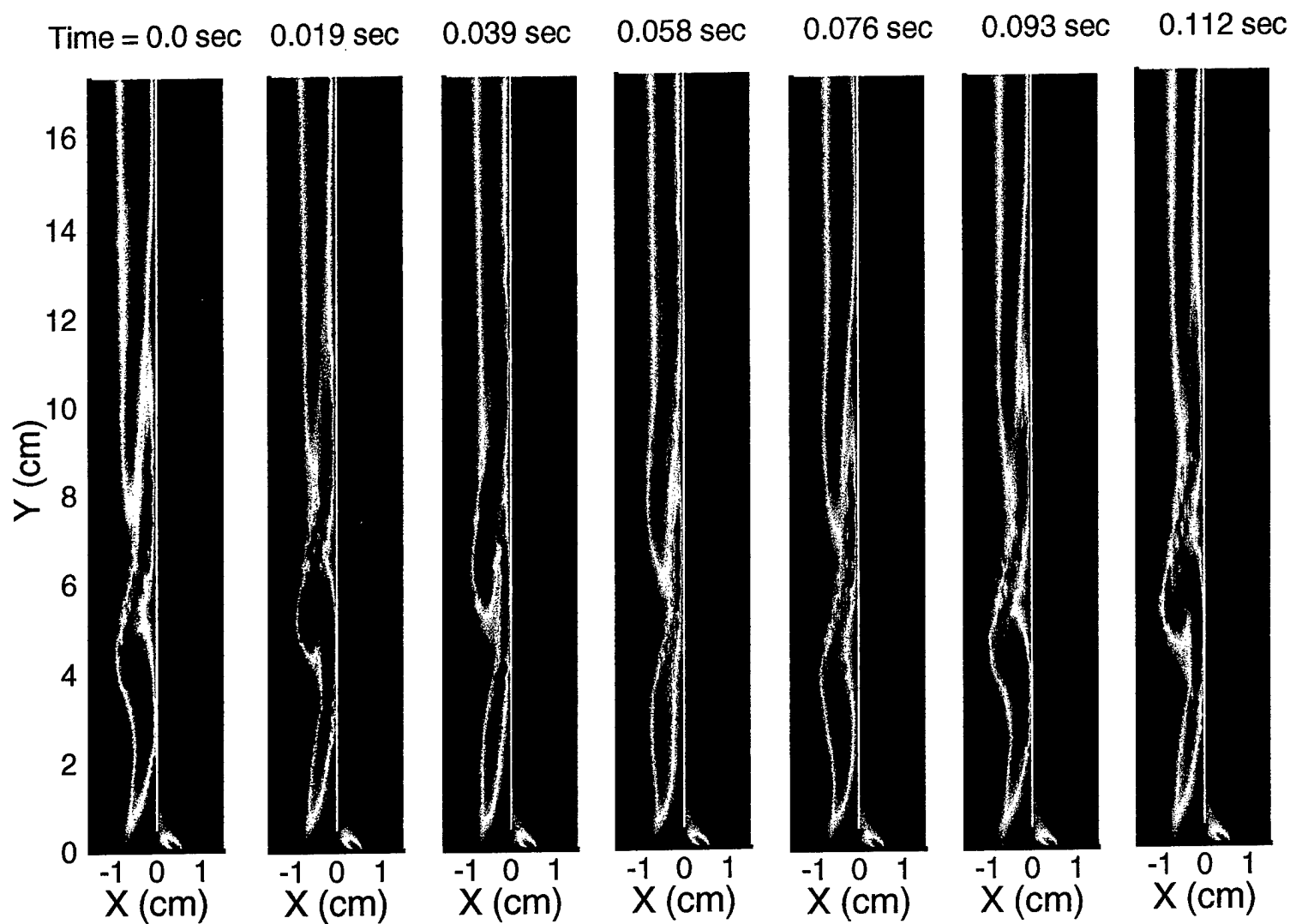
Fig. 4. Vorticity contours at different time levels, above a pulsating methanol liquid pool fire illustrating the puffing nature of the diffusion flame.
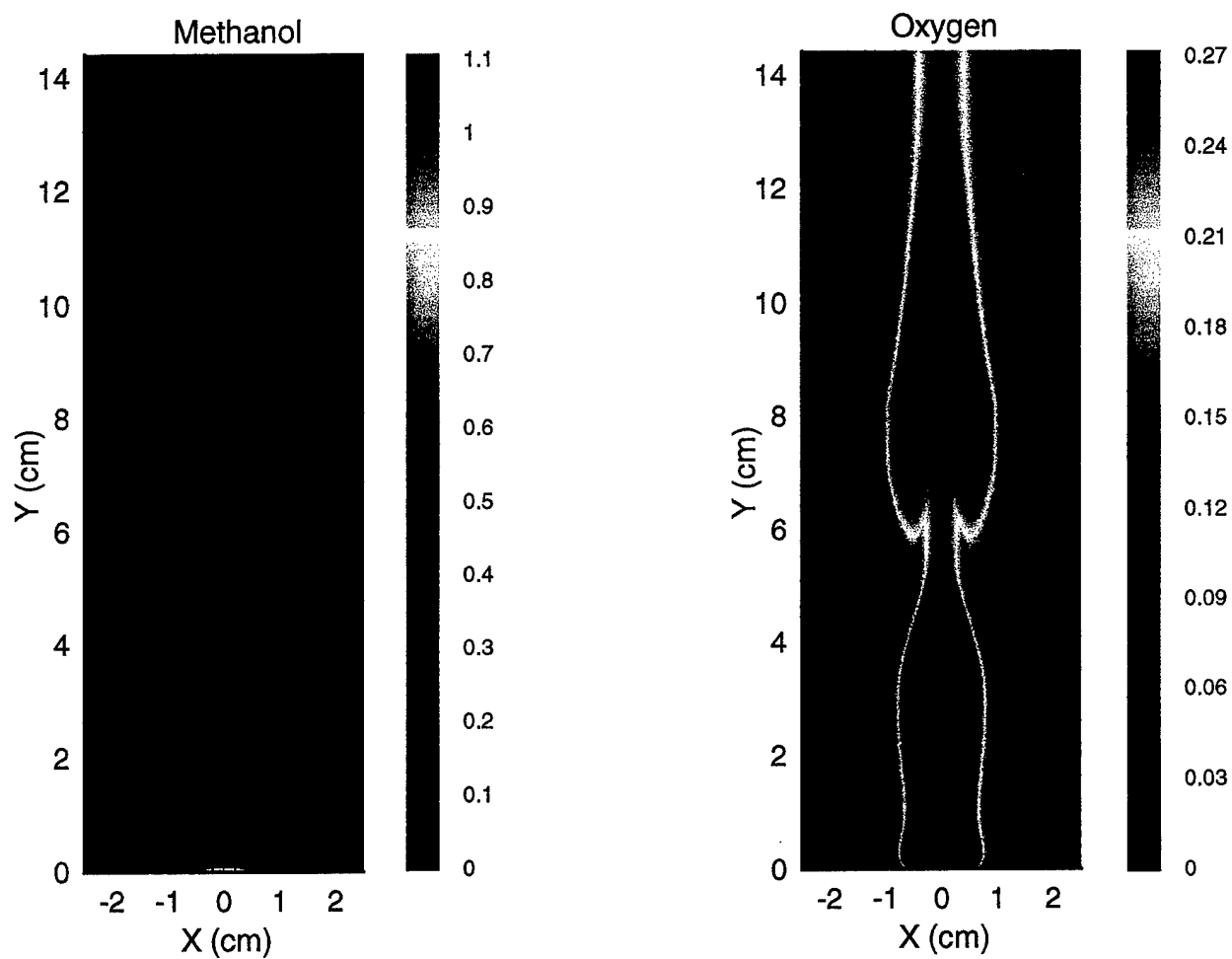
Fig. 5. Contours of major reactants, methanol gas and oxygen density (kg/m^3) above a methanol liquid pool fire.
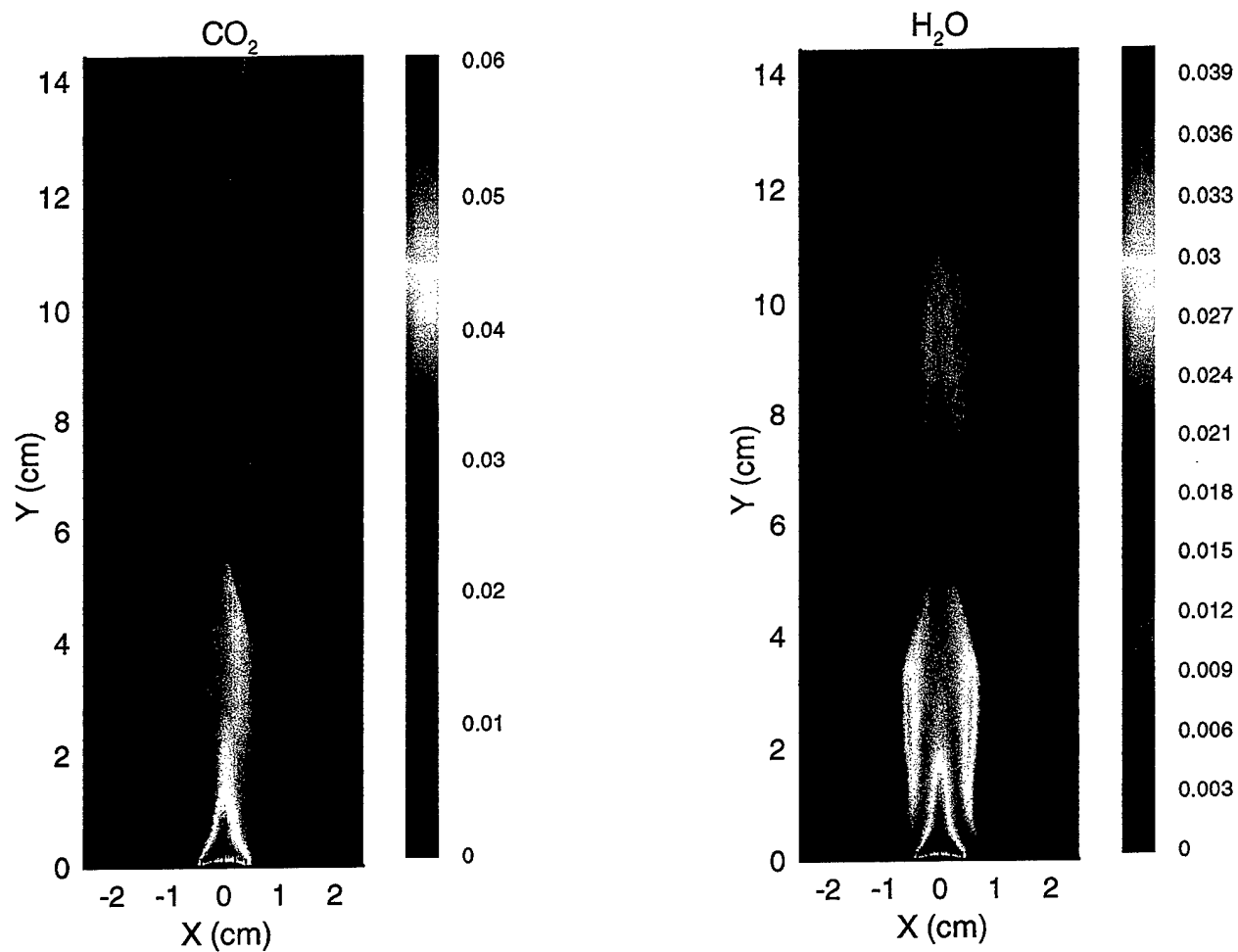
Fig. 6. Density distributions of major products, Carbon-dioxide and water vapor (kg/m^3) above a methanol liquid pool fire.
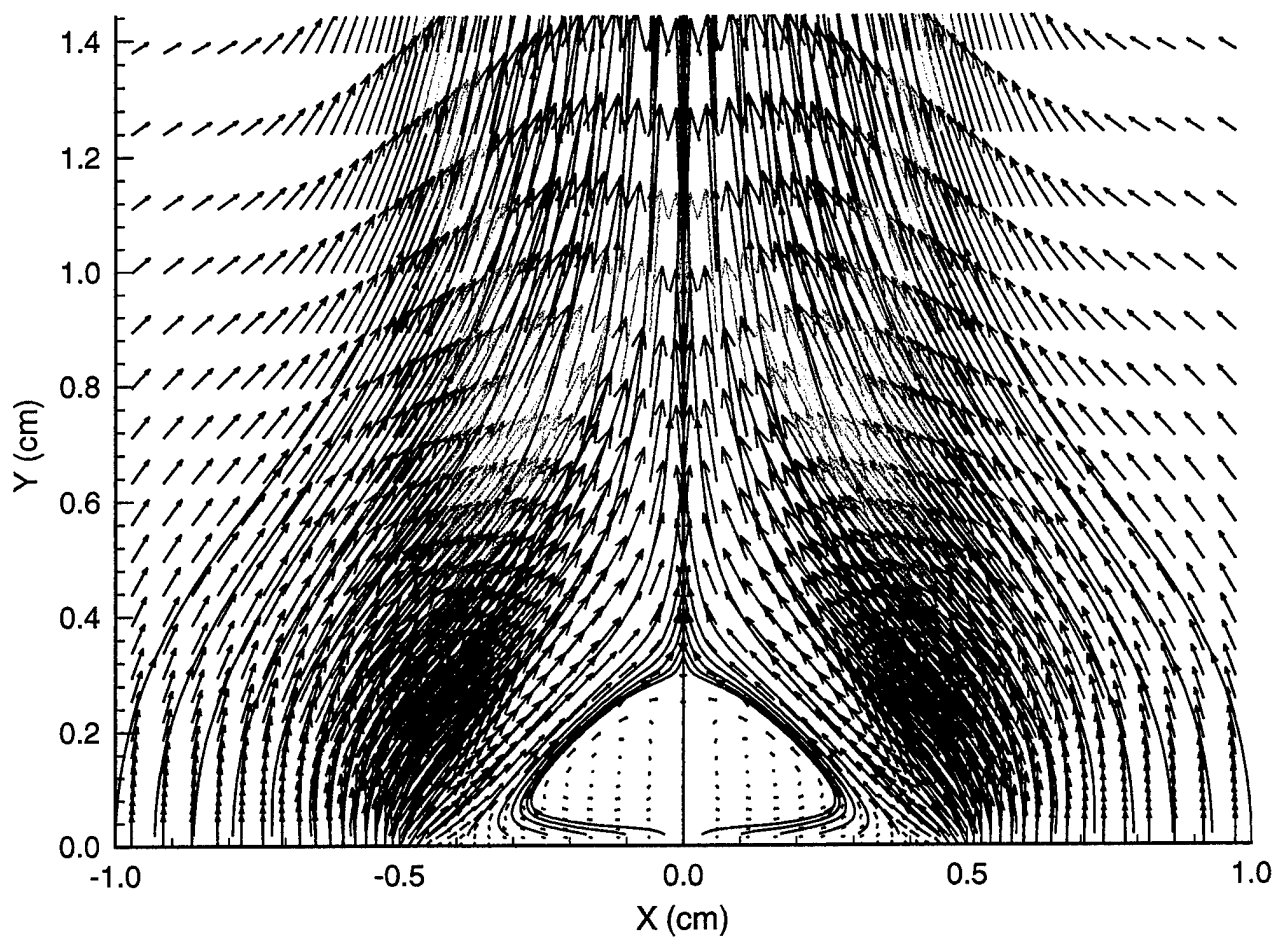
Fig. 7. Typical streamline and velocity vectors above a methanol liquid pool fire. The velocity vectors have been color coded with red showing the highest gas velocity and blue showing the lowest gas velocity. The streamline pattern (black) clearly indicate the entrainment of oxidizer into the diffusion flame.
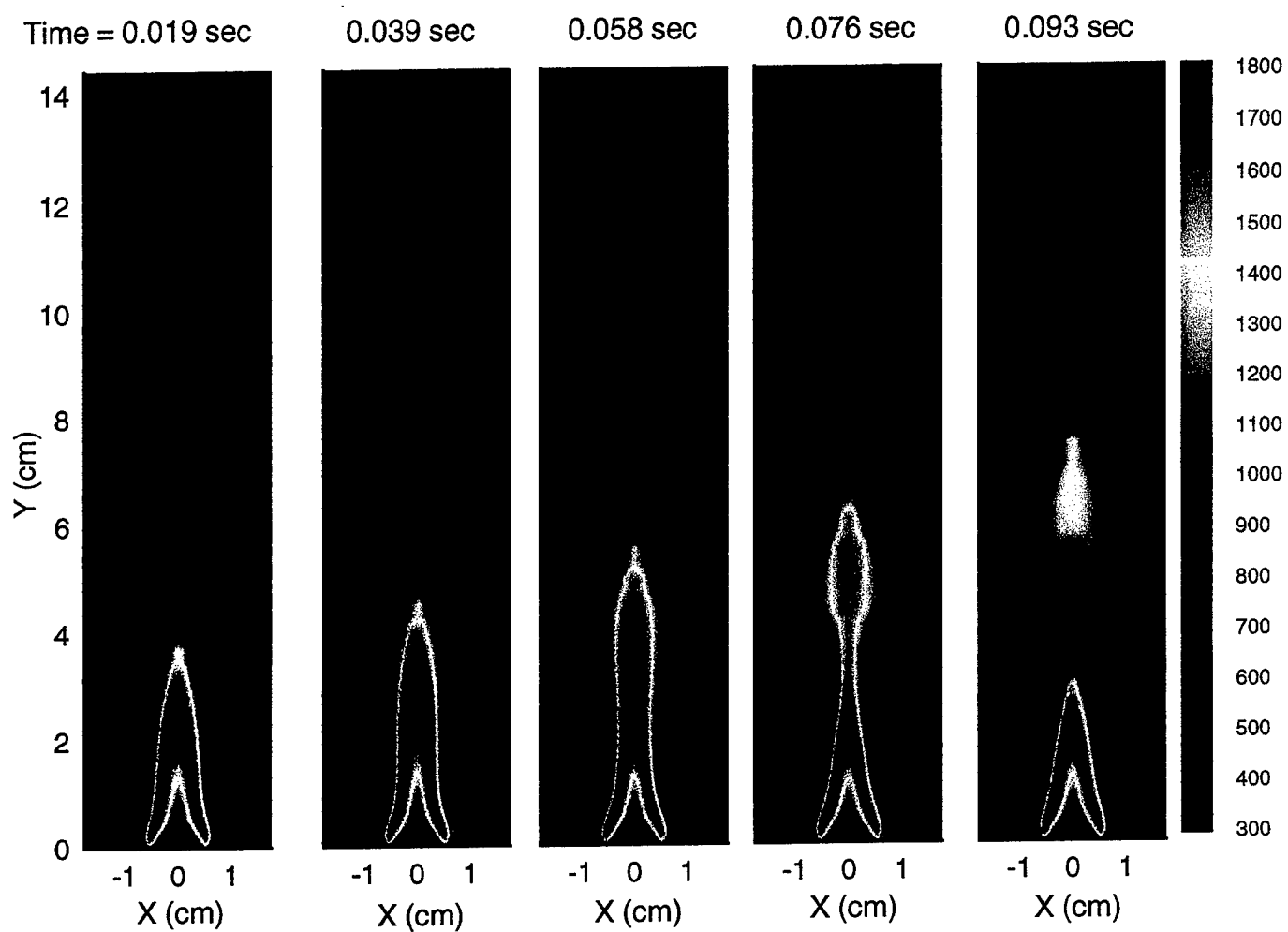
Fig. 8. Typical temperature contours (K) above a methanol liquid pool fire showing the pulsating nature of the diffusion flame.

Co-flow Velocity = 10 cm/sec
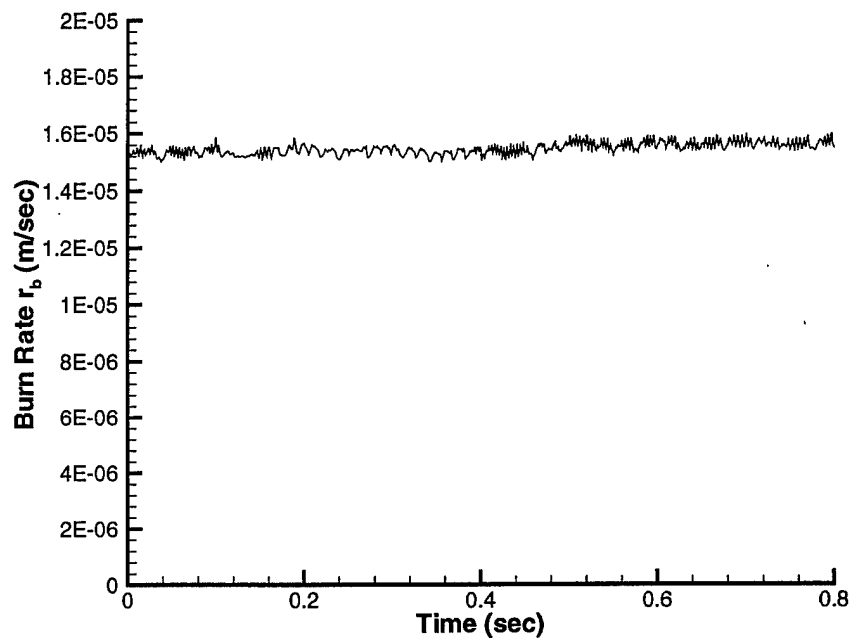
Co-flow Velocity = 2 cm/sec
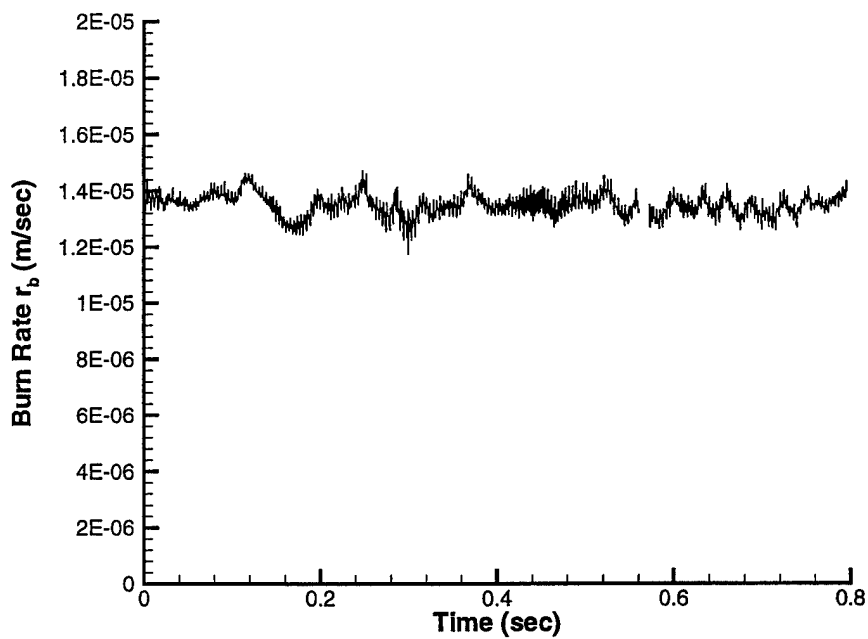
Fig. 9. Variation of burning rate as a function of time for co-flow air velocities of 10.0 *cm/sec* and 2.0 *cm/sec*.
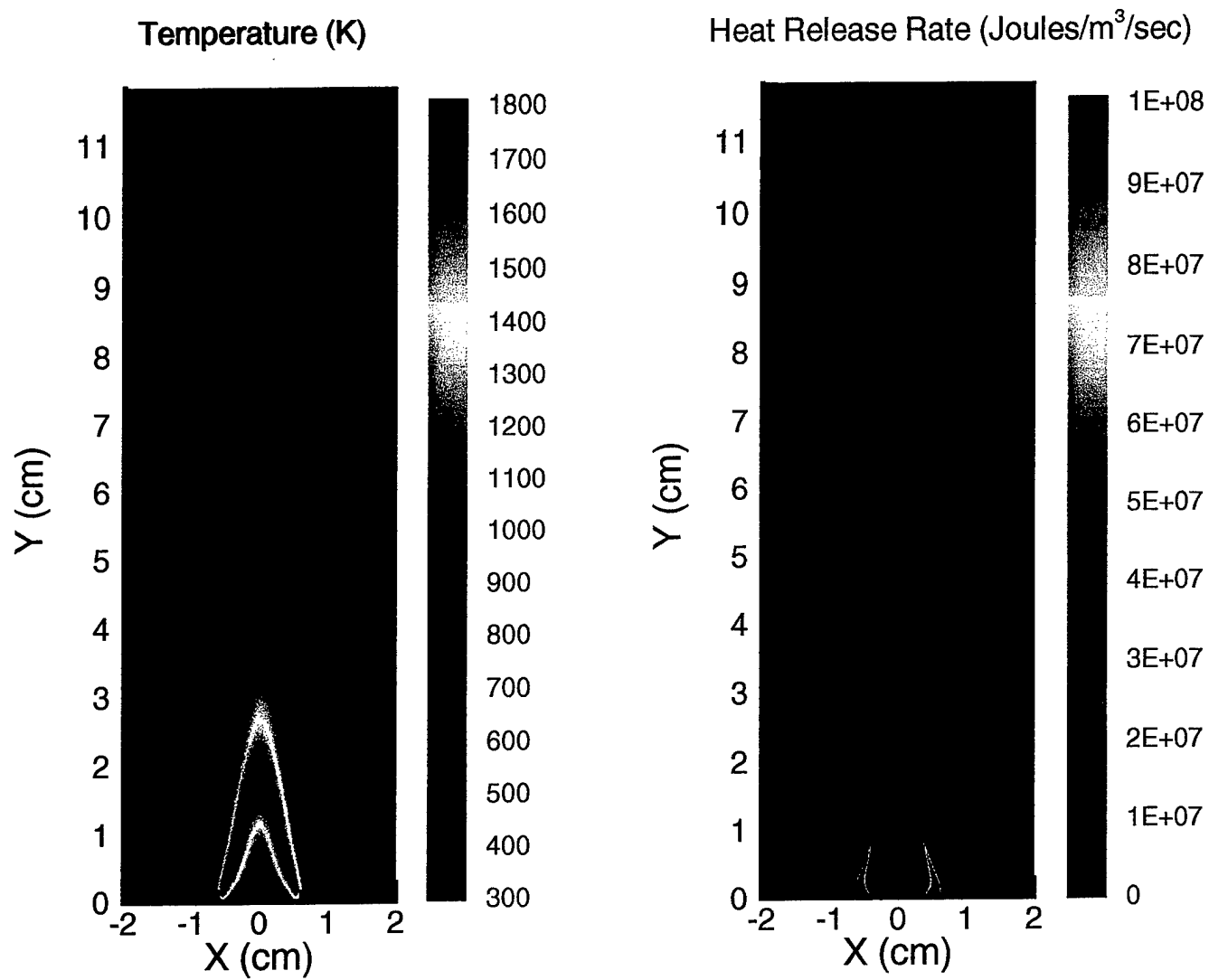
Fig. 10. Typical temperature and heat release rate contours above a methanol liquid pool fire with co-flow air velocity of 20*cm/sec*.
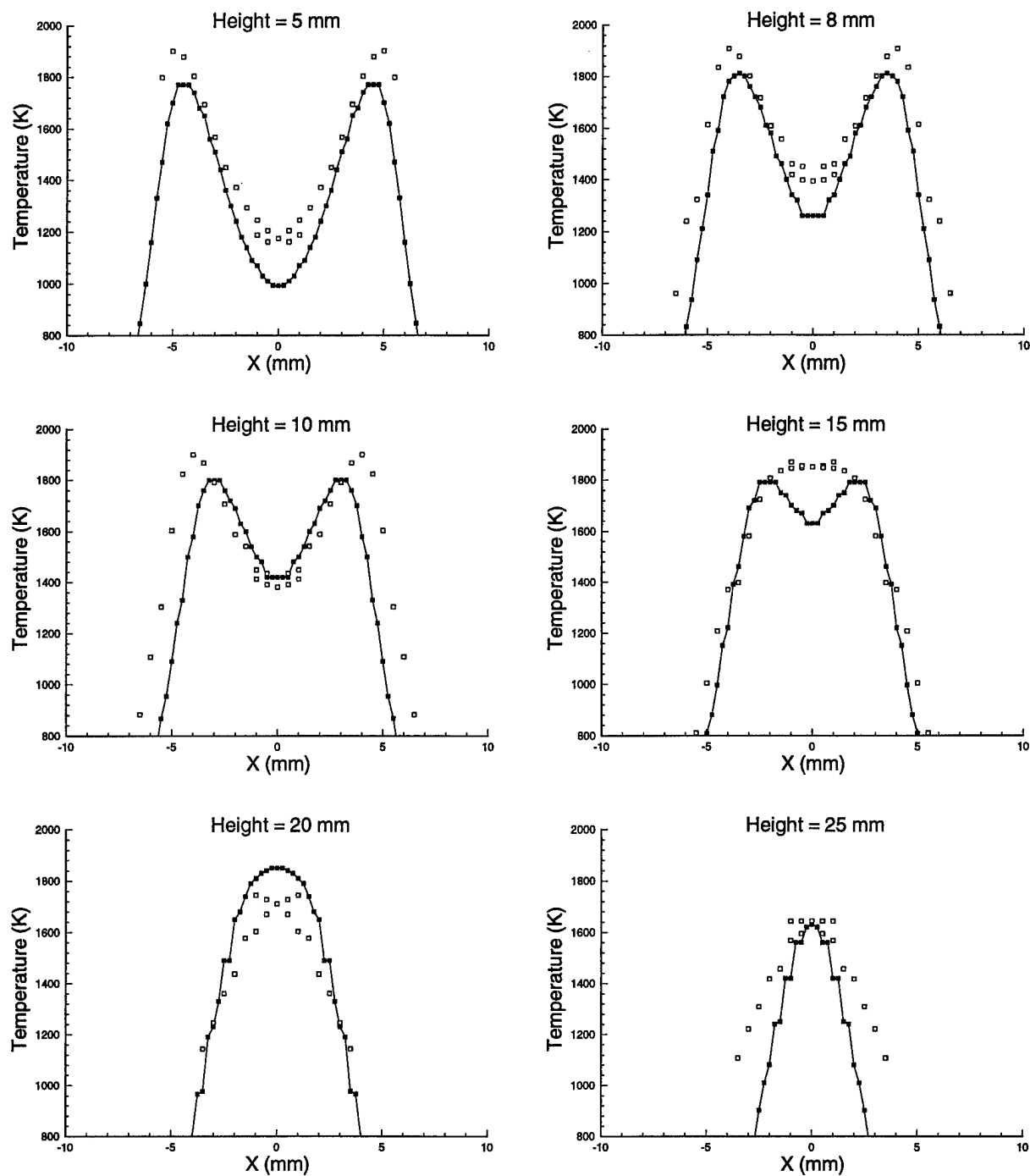
Fig. 11. Comparison between numerical and experimental results at various heights above the burner surface.
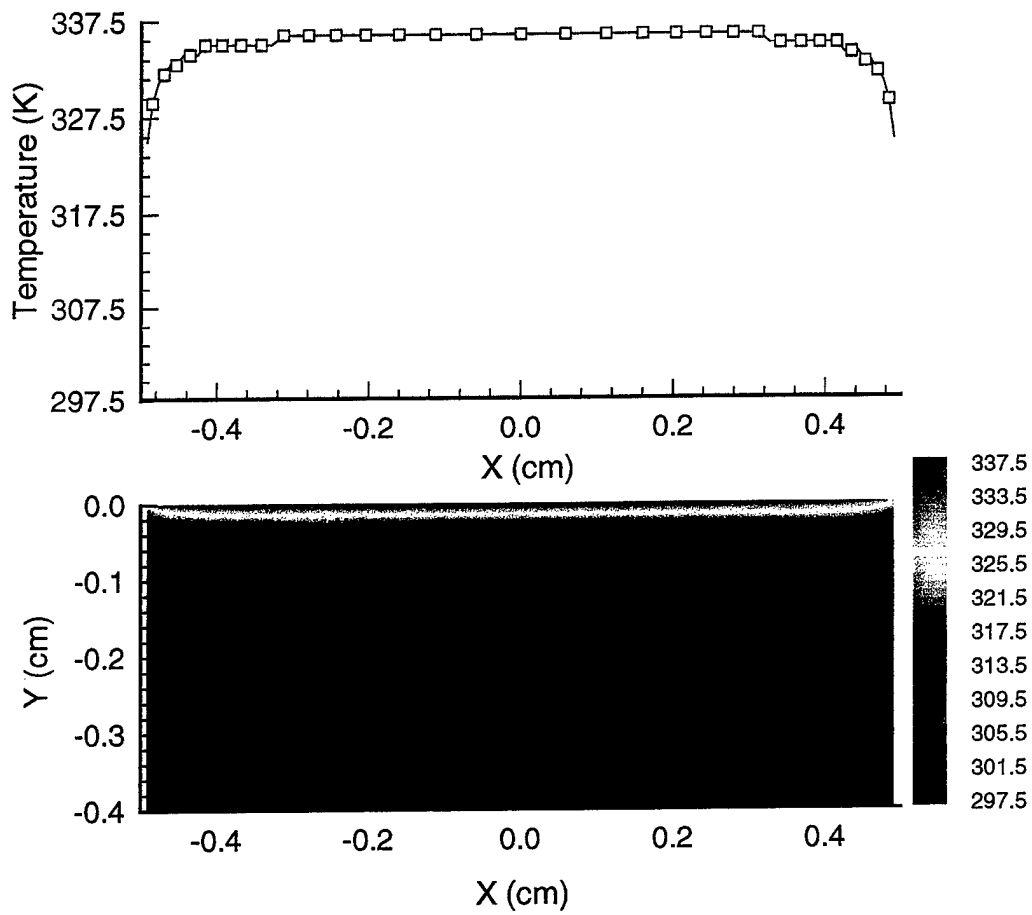
Fig. 12. Temperature contours in the liquid pool showing the structure of the thermal wave. Also shown is the variation of the surface temperature as a function of distance from the centerline.

Co-flow Air Velocity=40 cm/sec
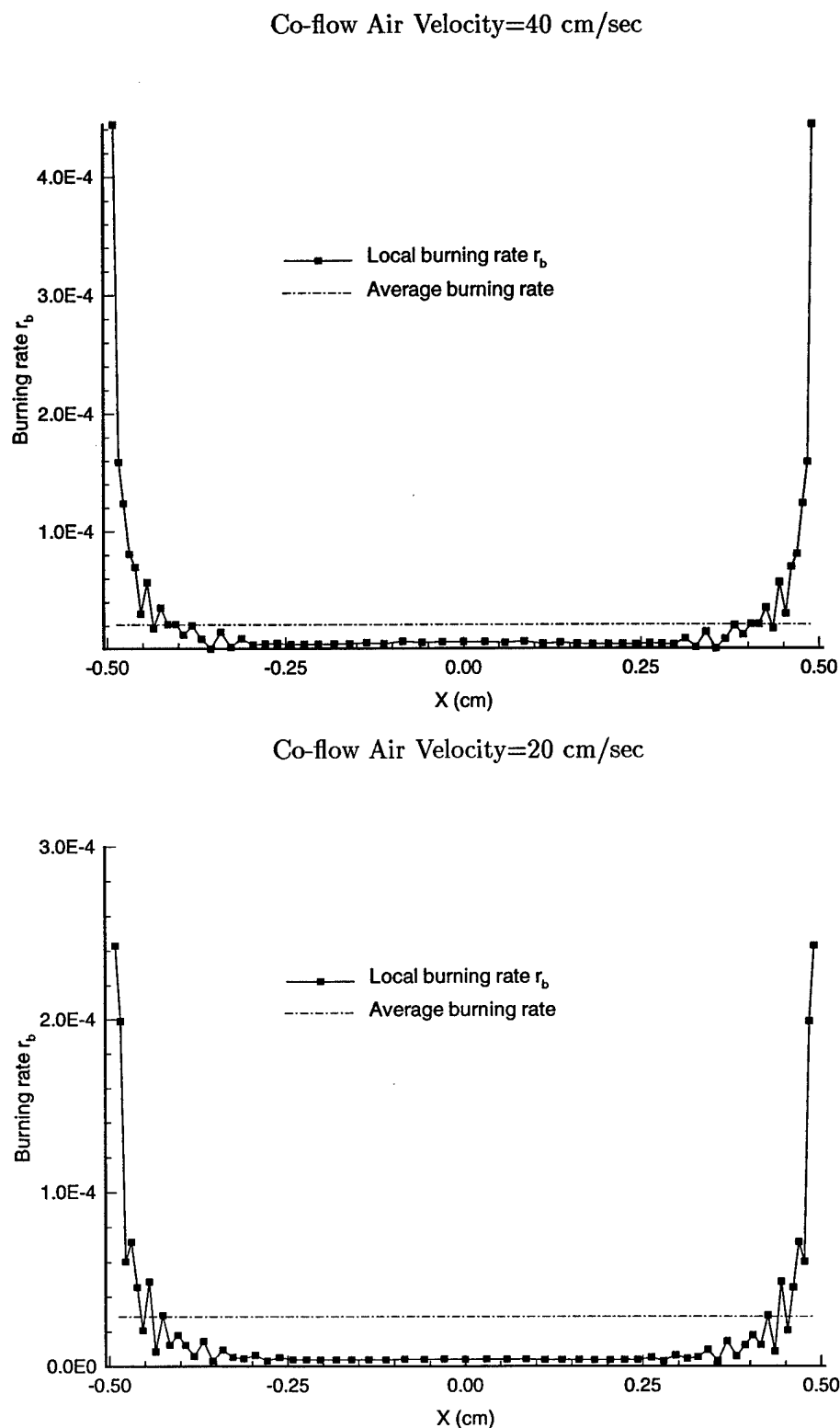

Co-flow Air Velocity=20 cm/sec

Fig. 13. Local regression rate (burning rate) as a function of distance from the centerline at the pool surface. Results shown are for two different co-flow air velocities of $40cm/sec$ and $20cm/sec$.
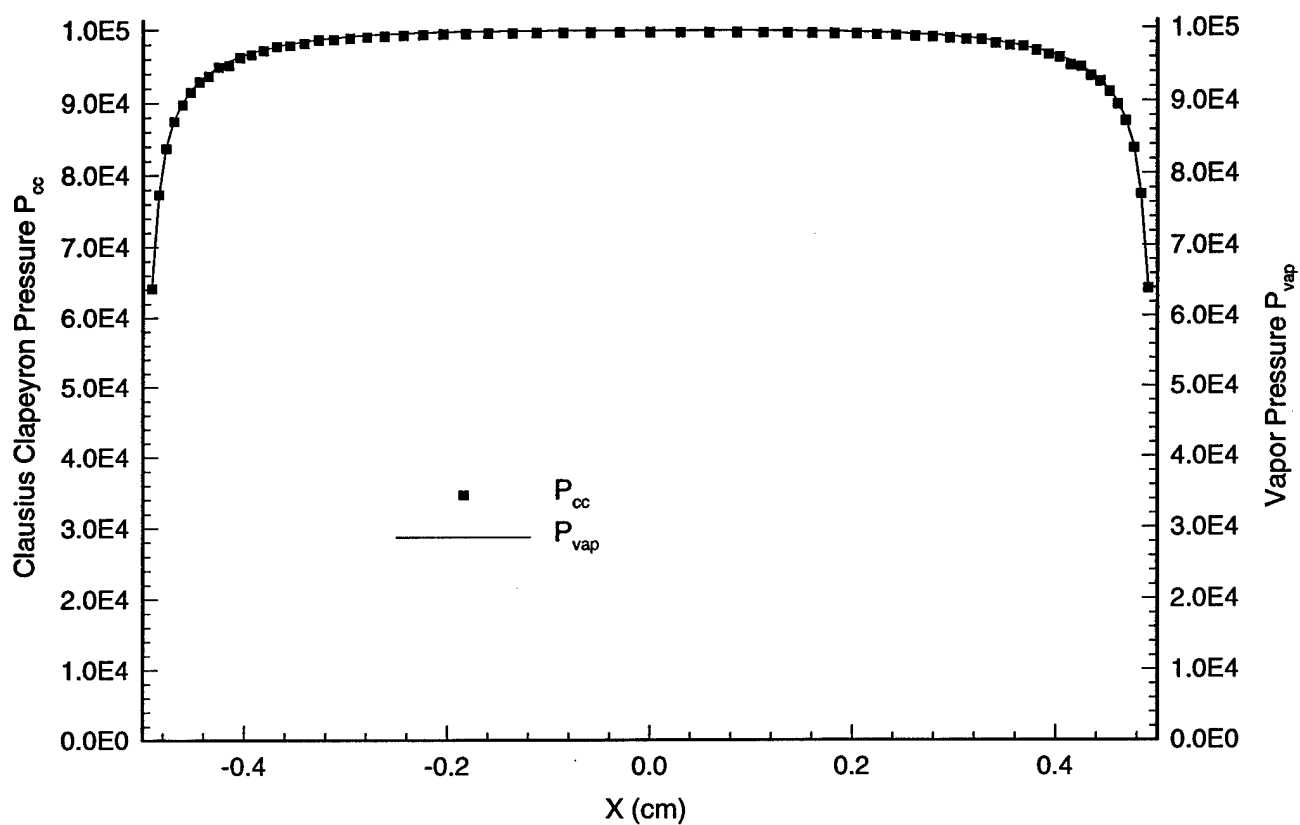
Fig. 14. Variation of the Clausius Clapeyron pressure and the vapor pressure as a function of distance along the burner surface.